

Stokes waves with constant vorticity: I. numerical computation

Sergey A. Dyachenko[†] and Vera Mikyoung Hur

Department of Mathematics, University of Illinois at Urbana-Champaign
Urbana, IL 61801 USA

(Received xx; revised xx; accepted xx)

Periodic traveling waves are numerically computed in a constant vorticity flow subject to the force of gravity. The Stokes wave problem is formulated via a conformal mapping as a nonlinear pseudo-differential equation, involving a periodic Hilbert transform for a strip, and solved by the Newton-GMRES method. It works well with a fast Fourier transform and is more effective than a boundary integral method. The result is in excellent agreement, qualitatively and quantitatively, with earlier ones.

For strong positive vorticity, in the finite or infinite depth, overhanging profiles are found as the steepness increases and tend to a touching wave, whose profile self-intersects somewhere along the trough line, trapping an air bubble; the numerical solutions become unphysical as the steepness increases further and make a gap in the wave speed versus steepness plane; a touching wave then takes over and the physical solutions follow in the wave speed versus steepness plane until they ultimately tend to an extreme wave, which exhibits a sharp corner at the crest. Overhanging waves of nearly maximum heights are found to approach rigid body rotation of a fluid disk as the strength of positive vorticity increases.

Key words: Stokes waves; constant vorticity; numerical; conformal

1. Introduction

Stokes (1847) (see also Stokes 1880) made many contributions about periodic waves at the surface of an incompressible inviscid fluid in two dimensions, subject to the force of gravity, traveling a long distance at a practically constant velocity without change of form. For instance, he observed that crests tend to sharpen and troughs flatter as the amplitude increases, and conjectured that the wave of greatest height exhibits a 120° corner at the crest. Amick *et al.* (1982) proved that a limiting wave exists, whose angle at the crest is 120° . In an irrotational flow of infinite depth, Stokes waves are much studied analytically and numerically. Some recent advances are based on the formulation of the problem as a nonlinear pseudo-differential equation, involving the periodic Hilbert transform — namely, the Babenko equation. For instance, Dyachenko *et al.* (2016); Lushnikov (2016); Lushnikov *et al.* (2017) numerically approximated the wave of greatest height and uncovered the structure of the singularities in meticulous detail.

The zero vorticity assumption may be justified in some situations. Moreover, in the absence of initial vorticity, boundaries or currents, water waves will have zero vorticity at all later times. But rotational effects are significant in many situations. For

[†] Email address for correspondence: sdyachen@illinois.edu

instance, in any region where wind blows, there is a surface drift of the water, and wave parameters, such as maximum wave height, are sensitive to the velocity at a wind-drift boundary layer. Moreover, currents produce shear at the bed of the sea or a river; see Teles da Silva & Peregrine (1988), for instance.

For arbitrary vorticity, Constantin & Strauss (2004) worked out the global bifurcation of Stokes waves in the finite depth, Hur (2006, 2011) in the infinite depth, and Ko & Strauss (2008*a,b*) numerically computed, assuming that there is no overhanging or internal stagnation. For zero vorticity, a Stokes wave is necessarily the graph of a single valued function and, moreover, the wave speed exceeds the directional particle velocity inside the fluid. But, even for constant vorticity, Simmen & Saffman (1985); Teles da Silva & Peregrine (1988); Ribeiro *et al.* (2017), among others, numerically observed overhanging profiles and interior stagnation points.

Constant vorticity is of particular interest because of its analytical tractability. Moreover, it is representative of a wide range of physical scenarios. When waves are short compared with the vorticity length scale, the vorticity at a surface layer is dominant in the wave dynamics. Moreover, when waves are long compared with the fluid depth, the mean vorticity is more important than its specific distribution; see Teles da Silva & Peregrine (1988), for instance. Examples include tidal currents — alternating lateral movements of water associated with the rise and fall of the tide — where positive or negative constant vorticity suitable for the ebb or flood, respectively; see Constantin *et al.* (2016), for instance.

Recently, Constantin *et al.* (2016) extended the Babenko equation, to permit constant vorticity and finite depth, and demonstrated the global bifurcation of Stokes waves. Moreover, they conjectured that at the boundary of the solution curve (in a suitable function space), one reaches: either an *extreme wave*, which exhibits a sharp corner at the crest and whose profile is single valued or overhanging, or a *touching wave*, whose profile self-intersects somewhere along the trough line, trapping an air bubble.

Simmen & Saffman (1985) used a boundary integral method and numerically computed Stokes waves in a constant vorticity flow of infinite depth. They found touching waves, among others, which is higher than the extreme wave for some vorticity. Moreover, they detected a *fold* in the wave speed versus steepness plane for some vorticity, which implies non-uniqueness. Teles da Silva & Peregrine (1988) extended the result in the finite depth. Vanden-Broeck (1996) located a branch of Stokes waves in the infinite depth, which tend to a closed region of fluid in rigid body rotation at the zero gravity limit.

Here we use a fast Fourier transform and the Newton-GMRES method, and numerically solve the extension of the Babenko equation, permitting constant vorticity and finite depth. The result is in excellent agreement, qualitatively and quantitatively, with those of Simmen & Saffman (1985); Teles da Silva & Peregrine (1988); Vanden-Broeck (1996), among others.

For negative or weak positive vorticity, in the finite or infinite depth, we learn that single valued profiles tend to an extreme wave as the steepness increases, like the well-known result for zero vorticity. But, for strong positive vorticity, we find that overhanging profiles appear as the steepness increases and tend to a touching wave; the numerical solutions become unphysical as the steepness increases further and make a *gap* in the wave speed versus steepness plane. By the way, the numerical method in Simmen & Saffman (1985), for instance, diverges in the gap. A touching wave then takes over and the physical solutions follow along a fold until they ultimately tend to an extreme wave, whose profile seems single valued. Moreover, we find that overhanging waves of nearly maximum heights approach rigid body rotation of a fluid disk as the strength of positive vorticity increases.

2. Formulation

The water wave problem, in the simplest form, concerns the wave motion at the surface of an incompressible inviscid fluid in two dimensions, lying below a body of air, and acted on by gravity. We assume for simplicity that the density = 1. Suppose for definiteness that in Cartesian coordinates, waves propagate in the x direction and gravity acts in the negative y direction. Suppose that the fluid occupies the region, bounded above by a free surface and below by the rigid bed $y = -h$ for some constant h in the range $(0, \infty]$. Let $y = \eta(x; t)$, $x \in \mathbb{R}$, represent the fluid surface at time t . We assume for now that η is single valued (but see the discussion following (2.15)). Let

$$\Omega(t) = \{(x, y) \in \mathbb{R}^2 : -h < y < \eta(x; t)\} \quad \text{and} \quad \Gamma(t) = \{(x, \eta(x; t)) : x \in \mathbb{R}\}.$$

Let $\mathbf{u} = \mathbf{u}(x, y; t)$ denote the velocity of the fluid at the point (x, y) and time t , and $p = p(x, y; t)$ the pressure. They satisfy the Euler equations for an incompressible fluid:

$$\mathbf{u}_t + (\mathbf{u} \cdot \nabla) \mathbf{u} = -\nabla p + (0, -g) \quad (2.1a)$$

and

$$\nabla \cdot \mathbf{u} = 0 \quad (2.1b)$$

in $\Omega(t)$, where g is the constant due to gravitational acceleration. Throughout, we express partial differentiation by a subscript, $\nabla = (\partial_x, \partial_y)$ and Δ the Laplacian. We assume that the vorticity

$$\omega := \nabla \times \mathbf{u} \quad (2.1c)$$

is constant. By the way, if vorticity is constant everywhere in the fluid at the initial time then it remains so at all later times, so long as the fluid region is two dimensional and simply connected.

The kinematic and dynamic conditions at the fluid surface:

$$\eta_t + \mathbf{u} \cdot \nabla(\eta - y) = 0 \quad \text{and} \quad p = p_{atm} \quad \text{at} \quad \Gamma(t) \quad (2.1d)$$

state, respectively, that the fluid particles do not invade the air, nor vice versa, and that the pressure at the fluid surface equals the constant atmospheric pressure = p_{atm} . Here we assume that the air is quiescent and neglect the effects of surface tension. In the finite depth, where $h < \infty$, the boundary condition at the fluid bed:

$$\mathbf{u} \cdot (0, -1) = 0 \quad \text{at} \quad y = -h \quad (2.1e)$$

states that the fluid particles at the bed remain so at all times. We assume in addition that the solutions of (2.1) are $2L$ periodic in the x variable for some L .

For any $\omega \in \mathbb{R}$, $h \in (0, \infty)$ and $c \in \mathbb{R}$, it is straightforward to verify that

$$\eta(x; t) = 0, \quad \mathbf{u}(x, y; t) = (-\omega y - c, 0) \quad \text{and} \quad p(x, y; t) = p_{atm} - gy, \quad (2.2)$$

where $x \in \mathbb{R}$ and $y \in (-h, 0)$, solve (2.1) at all times. They make a linear shear flow, for which the fluid surface is horizontal, the fluid velocity varies linearly in the y direction, and the pressure is hydrostatic. We assume that some external effects such as wind produce a flow of the kind and restrict the attention to the wave propagation in (2.2).

Suppose that

$$\mathbf{u}(x, y; t) = (-\omega y - c, 0) + \nabla \Phi(x, y; t) \quad \text{in} \quad \Omega(t), \quad (2.3)$$

whence (2.1b) implies that

$$\Delta \Phi = 0 \quad \text{in} \quad \Omega(t)$$

at all times. Namely, Φ is a velocity potential for the irrotational perturbation from (2.2). By the way, for arbitrary vorticity, the perturbation from the shear flow — not necessarily linear — becomes rotational, whence Φ is no longer viable to use. Let Ψ be a harmonic conjugate of Φ . Namely, Ψ is a stream function for the irrotational perturbation from (2.2). Clearly,

$$\mathbf{u} = (-\omega y - c, 0) + \nabla \times \Psi \quad (2.4)$$

and $\Delta\Psi = 0$ in $\Omega(t)$ at all times.

We substitute (2.3) and (2.4) into (2.1a), and we make an explicit calculation to arrive at

$$\Phi_t + \frac{1}{2}(\Phi_x^2 + \Phi_y^2) - (\omega y + c)\Phi_x + \omega\Psi + p - p_{atm} + gy = b(t)$$

for an arbitrary function $b(t)$. We substitute (2.3) and (2.4) into the other equations of (2.1), likewise. The result becomes

$$\Delta\Phi = 0 \quad \text{in } \Omega(t), \quad (2.5a)$$

$$\eta_t + (\Phi_x - \omega y - c)\eta_x = \Phi_y \quad \text{at } \Gamma(t), \quad (2.5b)$$

$$\Phi_t + \frac{1}{2}|\nabla\Phi|^2 - (\omega\eta + c)\Phi_x + \omega\Psi + g\eta = b(t) \quad \text{at } \Gamma(t) \quad (2.5c)$$

and

$$\Phi_y = 0 \quad \text{at } y = -h. \quad (2.5d)$$

Note that η and Φ, Ψ are $2L$ periodic in the x variable.

In the infinite depth, where $h = \infty$, we replace (2.5d) by

$$\Phi, \Psi \rightarrow 0 \quad \text{as } y \rightarrow -\infty \quad \text{uniformly for } x \in \mathbb{R}. \quad (2.5e)$$

Moreover, we may assume that $p \rightarrow p_{atm} - gy$ as $y \rightarrow -\infty$, whence $b(t) = 0$. But (2.3) implies that

$$\mathbf{u} \rightarrow (-\omega y - c, 0) \quad \text{as } y \rightarrow -\infty.$$

Therefore, nonzero constant vorticity in the infinite depth seems physically unrealistic. Nevertheless, (2.5) makes sense theoretically for any $h \in (0, \infty]$. Moreover, the infinite depth offers an auxiliary conformal mapping for effective numerical computation; see Section 4.2 and references therein for details. The effects of depth turn out to change the amplitude of a Stokes wave and other quantities, and they are insignificant otherwise. In stark contrast, the effects of constant vorticity are profound on limiting waves and other fundamental issues.

2.1. Reformulations via conformal mapping

We reformulate (2.5) via a conformal mapping of the fluid region from a strip, or from a half plane in the infinite depth. The idea traces back to Stokes (1880) in the steady wave setting and was explored in the unsteady wave setting by Ovsyannikov (1973) and, later, Meiron *et al.* (1981); Tanveer (1991, 1993); Zakharov *et al.* (2002), among others. Below, we proceed along the same line as the argument in Dyachenko *et al.* (1996a,b), but with suitable modifications to accommodate constant vorticity.

In what follows, we identify \mathbb{R}^2 with \mathbb{C} whenever it is convenient to do so.

Conformal mapping

Suppose that

$$z = z(w; t), \quad \text{where } w = u + iv \quad \text{and} \quad z = x + iy, \quad (2.6)$$

conformally maps

$$\Sigma_d := \{u + iv \in \mathbb{C} : -d < v < 0\}$$

of 2π period in the u variable to $\Omega(t)$ of $2L$ period in the x variable at time t for some d in the range $(0, \infty]$. Suppose that (2.6) extends to map $\{u + i0 : u \in \mathbb{R}\}$ to $\Gamma(t)$ and, moreover, $\{u - id : u \in \mathbb{R}\}$ to $\{x - ih : x \in \mathbb{R}\}$ if $d, h < \infty$, and $-i\infty$ to $-i\infty$ if $d, h = \infty$. Clearly, x and y enjoy the Cauchy-Riemann equations:

$$x_u = y_v \quad \text{and} \quad x_v = -y_u \quad (2.7)$$

in Σ_d . Moreover,

$$x(u + 2\pi + iv; t) = x(u + iv; t) + 2L \quad \text{and} \quad y(u + 2\pi + iv; t) = y(u + iv; t) \quad (2.8)$$

for $u + iv \in \overline{\Sigma_d}$.

Therefore, in the finite depth,

$$\Delta y = 0 \quad \text{in } \Sigma_d \quad \text{and} \quad y = -h \quad \text{at } v = -d.$$

Suppose that

$$y(u + i0; t) = \sum_{k \in \mathbb{Z}} \widehat{y}(k; t) e^{iku} \quad \text{for } u \in \mathbb{R} \quad (2.9)$$

in the Fourier series, where

$$\widehat{y}(k; t) = \frac{1}{2\pi} \int_{-\pi}^{\pi} y(u + i0; t) e^{iku} du,$$

whence

$$y(u + iv; t) = \frac{\widehat{y}(0; t) + h}{d} v + \widehat{y}(0; t) + \sum_{k \neq 0, \in \mathbb{Z}} \frac{\sinh(k(v + d))}{\sinh(kd)} \widehat{y}(k; t) e^{iku} \quad (2.10)$$

for $u + iv \in \overline{\Sigma_d}$. The Cauchy-Riemann equations imply

$$x(u + iv; t) = \frac{\widehat{y}(0; t) + h}{d} u - \sum_{k \neq 0, \in \mathbb{Z}} i \frac{\cosh(k(v + d))}{\sinh(kd)} \widehat{y}(k; t) e^{iku} \quad (2.11)$$

for $u + iv \in \overline{\Sigma_d}$ up to an additive constant. We infer from (2.11) and (2.10) that

$$x_u^2 + y_u^2 \neq 0 \quad \text{in } \overline{\Sigma_d}.$$

Moreover, we infer from (2.11) and the former equation of (2.8) that

$$\frac{L}{\pi} = \frac{\widehat{y}(0; t) + h}{d},$$

which relates the ‘‘mean conformal depth’’ d and the ‘‘mean fluid depth’’ h (see the discussion following (2.27)), depending on the solution of (2.6).

In what follows, we assume, without loss of generality, that $L = \pi$, whence the above simplifies to

$$d = \langle y \rangle + h, \quad (2.12)$$

where

$$\langle f \rangle = \frac{1}{2\pi} \int_{-\pi}^{\pi} f(u) du \quad (2.13)$$

is the mean over one period of a 2π periodic function f . Consequently, (2.11) simplifies

to

$$x(u + i0; t) = u - \sum_{k \neq 0} i \coth(kd) \widehat{y}(k; t) e^{iku} \quad \text{for } u \in \mathbb{R}. \quad (2.14)$$

Reformulation via conformal mapping

Recall (2.6), and let, by abuse of notation,

$$(x + iy)(u; t) = (x + iy)(u + i0; t) \quad \text{for } u \in \mathbb{R}. \quad (2.15)$$

Therefore,

$$y(u; t) = \eta(x(u; t); t).$$

In what follows, we allow that η be multi valued. By the way, one may extend (2.5) mutatis mutandis when the fluid surface is the trajectory of a parametric curve. A chain rule calculation reveals that

$$y_u = \eta_x x_u \quad \text{and} \quad y_t = \eta_x x_t + \eta_t.$$

Recall (2.3) and (2.4), and let

$$(\phi + i\psi)(w; t) = (\Phi + i\Psi)(z(w; t); t) \quad \text{for } w \in \Sigma_d. \quad (2.16)$$

Namely, $\phi + i\psi$ is a conformal velocity potential for the irrotational perturbation from (2.2). Since $\Phi + i\Psi$ is holomorphic in $\Omega(t)$ and since $z : \Sigma_d \rightarrow \Omega(t)$ is conformal, ϕ and ψ enjoy the Cauchy-Riemann equations:

$$\phi_u = \psi_v \quad \text{and} \quad \phi_v = -\psi_u \quad (2.17)$$

in Σ_d . A chain rule calculation and (2.7), (2.17) reveal that

$$\begin{pmatrix} \Phi_x \\ \Phi_y \end{pmatrix} = \frac{1}{x_u y_u - x_v y_v} \begin{pmatrix} y_v & -y_u \\ -x_v & x_u \end{pmatrix} \begin{pmatrix} \phi_u \\ \phi_v \end{pmatrix} = \frac{1}{x_u^2 + y_u^2} \begin{pmatrix} x_u & -y_u \\ y_u & x_u \end{pmatrix} \begin{pmatrix} \phi_u \\ -\psi_u \end{pmatrix},$$

where $x_u^2 + y_u^2 \neq 0$ in $\overline{\Sigma_d}$ by (2.11) and (2.10). Moreover, $\phi_t = \overline{\Phi}_x x_t + \overline{\Phi}_y y_t + \overline{\Phi}_t$. Let, by abuse of notation,

$$(\phi + i\psi)(u; t) = (\phi + i\psi)(u + i0; t) \quad \text{for } u \in \mathbb{R}. \quad (2.18)$$

We substitute (2.15) and (2.18) into (2.5b) and (2.5c), and we use the result from the chain rule calculations to arrive at

$$x_u y_t - y_u x_t + \psi_u - (\omega y + c) y_u = 0 \quad (2.19a)$$

and

$$\begin{aligned} \phi_t - \frac{1}{x_u^2 + y_u^2} ((x_u x_t + y_u y_t) \phi_u + (y_u x_t - x_u y_t) \psi_u \\ + \frac{1}{2} (\phi_u^2 + \psi_u^2) - (\omega y + c) (x_u \phi_u + y_u \psi_u)) + \omega \psi + g y - b(t) = 0 \end{aligned} \quad (2.19b)$$

at $v = 0$. Note that

$$\Delta y, \Delta \phi = 0 \quad \text{in } \Sigma_d. \quad (2.19c)$$

Note that

$$y = -h \quad \text{and} \quad \phi_v = 0 \quad \text{at } v = -d \quad \text{if } d, h < \infty \quad (2.19d)$$

by (2.5d), and

$$\phi, \psi \rightarrow 0 \quad \text{as } v \rightarrow -\infty \quad \text{uniformly for } u \in \mathbb{R} \quad \text{if } d, h = \infty \quad (2.19e)$$

by (2.5e) and (2.16). Moreover, y and ϕ , ψ are 2π periodic in the u variable. Therefore, (2.19) is to rewrite (2.5).

Below, we relate x to y and ϕ to ψ at the face of Σ_d , whereby we reformulate (2.19) and, hence, (2.5) for $y = y(u; t)$ and $\phi = \phi(u; t)$. It makes use of periodic Hilbert transforms for a strip.

Periodic Hilbert transforms for a strip

For d in the range $(0, \infty)$, let \mathcal{H}_d and \mathcal{T}_d denote Fourier multiplier operators, defined in the periodic setting as

$$\mathcal{H}_d e^{iku} = -i \tanh(kd) e^{iku} \quad \text{for } k \in \mathbb{Z}$$

and

$$\mathcal{T}_d e^{iku} = \begin{cases} -i \coth(kd) e^{iku} & \text{if } k \neq 0, \in \mathbb{Z}, \\ 0 & \text{if } k = 0. \end{cases} \quad (2.20)$$

Clearly,

$$\mathcal{H}_d \mathcal{T}_d = \mathcal{T}_d \mathcal{H}_d = -1 \quad \text{if } k \neq 0. \quad (2.21)$$

As $d \rightarrow \infty$, at least formally, \mathcal{H}_d and \mathcal{T}_d tend to the periodic Hilbert transform, defined likewise as

$$\mathcal{H} e^{iku} = -i \operatorname{sgn}(k) e^{iku} \quad \text{for } k \in \mathbb{Z}.$$

Among other properties of \mathcal{H}_d and \mathcal{T}_d , of particular importance for the present purpose is that the ‘‘Titchmarsh theorem’’ (see Titchmarsh 1986, Theorem 95, for instance) or the Sokhotski-Plemelj theorem (see Plemelj 1964; Gakhov 1990, for instance) extends, and \mathcal{H}_d and \mathcal{T}_d relate the real part of a holomorphic and 2π periodic function in a strip to the imaginary part at the face of the strip, and vice versa. If $F = F(u + iv)$ is holomorphic in the lower half plane of \mathbb{C} and if F vanishes sufficiently rapidly as $v \rightarrow -\infty$ then the Titchmarsh theorem states that the real and imaginary parts of $F(\cdot + i0)$ are the Hilbert transforms of each other. For any $d \in (0, \infty)$, likewise, if F is holomorphic in Σ_d and 2π periodic in the u variable and if $\operatorname{Re} F(u + i0) = f(u)$ and $(\operatorname{Re} F)_v(u - id) = 0$ for $u \in \mathbb{R}$ then

$$F(u + i0) = (1 - i\mathcal{H}_d)f(u) \quad \text{for } u \in \mathbb{R} \quad (2.22)$$

up to an additive imaginary constant. In other words, $1 - i\mathcal{H}_d$ makes the face value of a holomorphic and 2π periodic function in Σ_d , the normal derivative of whose real part vanishes at the bottom of Σ_d . Moreover, if F is holomorphic in Σ_d and 2π periodic in the u variable, if $\operatorname{Im} F(u + i0) = f(u)$ and $\operatorname{Im} F(u - id) = 0$ for $u \in \mathbb{R}$, and if $\langle f \rangle = 0$ in addition, where we employ the notation of (2.13), then

$$F(u + i0) = (\mathcal{T}_d + i)f(u) \quad \text{for } u \in \mathbb{R} \quad (2.23)$$

up to an additive real constant. In other words, $\mathcal{T}_d + i$ is the face value of a holomorphic and 2π periodic function in Σ_d , whose imaginary part is of mean zero at the face of Σ_d and vanishes at the bottom.

Implicit form

Returning to the water wave problem, in the finite depth, since $\phi + i\psi$ is holomorphic in Σ_d and satisfies (2.19d), we employ an extension of the Titchmarsh theorem to a strip (see (2.22)) to show that

$$(\phi + i\psi)(u; t) = (1 - i\mathcal{H}_d)\phi(u; t) \quad (2.24)$$

up to an additive imaginary constant. Moreover, we use (2.9), (2.14) and (2.20) to show that

$$(x + iy)(u; t) = u + (\mathcal{T}_d + i)y(u; t). \quad (2.25)$$

By the way, an extension of the Titchmarsh theorem (see (2.23)) does not apply to $x + iy$ because y needs not be of mean zero at the face of Σ_d . (See the discussion following (2.27).) In the infinite depth, the Titchmarsh theorem implies (2.24) and (2.25), where the periodic Hilbert transform replaces \mathcal{H}_d and \mathcal{T}_d .

To proceed, in the finite depth, we substitute (2.24) and (2.25) into (2.19a) and (2.19b), to arrive at

$$(1 + \mathcal{T}_d y_u) y_t - y_u \mathcal{T}_d y_t - \mathcal{H}_d \phi_u - (\omega y + c) y_u = 0 \quad (2.26a)$$

and

$$\begin{aligned} & ((1 + \mathcal{T}_d y_u)^2 + y_u^2)(\phi_t + g y - \omega \mathcal{H}_d \phi - b(t)) \\ & - ((1 + \mathcal{T}_d y_u) \mathcal{T}_d y_t + y_u y_t) \phi_u + (y_u \mathcal{T}_d y_t - (1 + \mathcal{T}_d y_u) y_t) \mathcal{H}_d \phi_u \\ & + \frac{1}{2}(\phi_u^2 + (\mathcal{H}_d \phi_u)^2) - (\omega y + c)((1 + \mathcal{T}_d y_u) \phi_u - y_u \mathcal{H}_d \phi_u) = 0. \end{aligned} \quad (2.26b)$$

Note that $y = y(u; t)$ and $\phi = \phi(u; t)$ are 2π periodic in the u variable. We claim that (2.26) is equivalent to (2.19) and, hence, (2.5), provided that d and h are related by (2.12). Indeed, y and ϕ extend as the imaginary and real parts of holomorphic and 2π periodic functions in Σ_d , which satisfy (2.19d). In the infinite depth, (2.26) is equivalent to (2.19) and, hence, (2.5), likewise, where the periodic Hilbert transform replaces \mathcal{H}_d and \mathcal{T}_d . Moreover, in an irrotational flow, (2.26) agrees with what Dyachenko *et al.* (1996a,b), for instance, derived.

We integrate (2.26a) over the periodic interval $[-\pi, \pi]$ and use that \mathcal{T}_d is anti-self-adjoint, to show that

$$\frac{d}{dt} \langle y(1 + \mathcal{T}_d y_u) \rangle = 0. \quad (2.27)$$

Therefore, if we locate the coordinates of the fluid region so that $\langle y(1 + \mathcal{T}_d y_u) \rangle = 0$ at the initial time then it remains so at all later times; y then measures the fluid surface displacement from zero and h the mean fluid depth. In the infinite depth, the periodic Hilbert transform replaces \mathcal{T}_d .

Explicit form

Concluding the reformulations, we solve (2.26) for y_t and ϕ_t explicitly.

In the finite depth, since z is holomorphic in Σ_d and since $|z_u|^2 \neq 0$ in $\overline{\Sigma_d}$ by (2.11) and (2.10), z_t/z_u is holomorphic in Σ_d . Note that

$$\operatorname{Im} \frac{z_t}{z_u} = \frac{x_u y_t - y_u x_t}{|z_u|^2} = \frac{\mathcal{H}_d \phi_u + (\omega y + c) y_u}{|z_u|^2} =: \frac{-\chi_u}{|z_u|^2} \quad \text{at } v = 0 \quad (2.28)$$

by (2.19a) and (2.24), and $\operatorname{Im}(z_t/z_u) = 0$ at $v = -d$ by (2.19d). By the way,

$$\chi = \psi - \left(\frac{1}{2}\omega y^2 + cy\right) \quad (2.29)$$

makes a conformal stream function by (2.4) and (2.16). Note that $\langle \operatorname{Im}(z_t/z_u) \rangle = 0$ for all $v \in [-d, 0]$ by the Cauchy-Riemann equations and (2.19d). Therefore, an extension of the Titchmarsh theorem to a strip (see (2.23)) implies that

$$\frac{z_t}{z_u} = (\mathcal{T}_d + i) \left(\frac{-\chi_u}{|z_u|^2} \right) \quad \text{at } v = 0.$$

Or, equivalently,

$$x_t = ((1 + \mathcal{T}_d y_u) \mathcal{T}_d - y_u) \left(\frac{-\chi_u}{|z_u|^2} \right) \quad \text{and} \quad y_t = (1 + \mathcal{T}_d y_u + y_u \mathcal{T}_d) \left(\frac{-\chi_u}{|z_u|^2} \right) \quad \text{at } v = 0. \quad (2.30)$$

Moreover,

$$\operatorname{Re} \frac{z_t}{z_u} = \frac{x_u x_t + y_u y_t}{|z_u|^2} = \mathcal{T}_d \left(\frac{-\chi_u}{|z_u|^2} \right) \quad \text{at } v = 0. \quad (2.31)$$

We substitute (2.28) and (2.31) into (2.19b), to arrive at

$$\begin{aligned} \phi_t + \phi_u \mathcal{T}_d \left(\frac{\chi_u}{|z_u|^2} \right) - \frac{1}{|z_u|^2} \left(\frac{1}{2} (\phi_u^2 - \psi_u^2) (\omega y + c) (1 + \mathcal{T}_d y_u) \phi_u \right) \\ - \omega \mathcal{H}_d \phi + g y - b(t) = 0 \quad \text{at } v = 0. \end{aligned} \quad (2.32)$$

But an extension of the Titchmarsh theorem to a strip (see (2.22)) implies that

$$(\phi_u - i \mathcal{H}_d \phi_u)^2 = \phi_u^2 - (\mathcal{H}_d \phi_u)^2 - 2i \phi_u \mathcal{H}_d \phi_u$$

is the face value of the holomorphic and 2π periodic function $= (\phi_u + i \psi_u)^2$ in Σ_d , the normal derivative of whose real part vanishes at the bottom of Σ_d by the Cauchy-Riemann equations and (2.19d). It then follows from (2.22) and (2.21) that

$$\phi_u^2 - (\mathcal{H}_d \phi_u)^2 = -2 \mathcal{T}_d (\phi_u \mathcal{H}_d \phi_u).$$

We substitute (2.29), (2.25), (2.24) and the above into the latter equation of (2.30) and (2.32), to arrive at

$$y_t = (1 + \mathcal{T}_d y_u + y_u \mathcal{T}_d) \left(\frac{\mathcal{H}_d \phi_u + (\omega y + c) y_u}{(1 + \mathcal{T}_d y_u)^2 + y_u^2} \right)$$

and

$$\begin{aligned} \phi_t = & -\phi_u \mathcal{T}_d \left(\frac{\mathcal{H}_d \phi_u + (\omega y + c) y_u}{(1 + \mathcal{T}_d y_u)^2 + y_u^2} \right) \\ & + \frac{1}{(1 + \mathcal{T}_d y_u)^2 + y_u^2} (\mathcal{T}_d (\phi_u \mathcal{H}_d \phi_u) + (\omega y + c) (1 + \mathcal{T}_d y_u) \phi_u) + \omega \mathcal{H}_d \phi - g y + b(t). \end{aligned} \quad (2.33)$$

Note that $y = y(u; t)$ and $\phi = \phi(u; t)$ are 2π periodic in the u variable. Clearly, (2.33) is equivalent to (2.19) and, hence, (2.26). Therefore, (2.33) is to solve (2.26) for y_t and ϕ_t explicitly. In the infinite depth, (2.33) is equivalent to (2.19) and, hence, (2.26), likewise, where the periodic Hilbert transform replaces \mathcal{H}_d and \mathcal{T}_d . Moreover, in an irrotational flow, (2.33) agrees with what Dyachenko *et al.* (1996a,b), for instance, derived.

2.2. The Stokes wave problem

We turn the attention to the solutions of (2.33), for which $y_t, \phi_t = 0$ and $b(t) = \text{constant}$, and, hence, the steady solutions of (2.5). They make Stokes waves, permitting constant vorticity and finite depth.

In what follows, the prime means ordinary differentiation in the u variable.

Formulation via conformal mapping

In the finite depth, we substitute $y_t = 0$ into the latter equation of (2.30) to arrive at

$$\psi' = \omega y y' + c y' \quad \text{at } v = 0. \quad (2.34)$$

Indeed, $(1 + \mathcal{T}_d y')^2 + (y')^2 \neq 0$ pointwise in \mathbb{R} by (2.25) and (2.14), (2.9). By the way, (2.34) states that the fluid surface itself makes a streamline. Note from (2.24) and (2.21) that

$$\phi' = \mathcal{T}_d(\omega y y' + c y') \quad \text{at } v = 0. \quad (2.35)$$

Moreover, we substitute $\phi_t = 0$ into (2.32) and use (2.34) and (2.35), to arrive at

$$\begin{aligned} & (\mathcal{T}_d(\omega y y' + c y'))^2 - (\omega y y' + c y')^2 - 2(\omega y + c)(1 + \mathcal{T}_d y')\mathcal{T}_d(\omega y y' + c y') \\ & + 2\omega((1 + \mathcal{T}_d y')^2 + (y')^2)(\frac{1}{2}\omega y^2 + c y) - 2(b - g y)((1 + \mathcal{T}_d y')^2 + (y')^2) = 0 \quad \text{at } v = 0 \end{aligned}$$

for some constant $b \in \mathbb{R}$. After a lengthy but straightforward calculation, it simplifies to

$$(c + \omega y(1 + \mathcal{T}_d y') - \omega \mathcal{T}_d(y y'))^2 = (c^2 + 2b - 2g y)((1 + \mathcal{T}_d y')^2 + (y')^2). \quad (2.36)$$

Or, equivalently,

$$y = \frac{1}{2g} \left(c^2 + 2b - \frac{(c + \omega y(1 + \mathcal{T}_d y') - \omega \mathcal{T}_d(y y'))^2}{(1 + \mathcal{T}_d y')^2 + (y')^2} \right). \quad (2.37)$$

In the infinite depth, the periodic Hilbert transform replaces \mathcal{T}_d . Therefore, the Stokes wave problem, permitting constant vorticity and finite depth, is to find $\omega \in \mathbb{R}$, $d \in (0, \infty]$, $b, c \in \mathbb{R}$ and a 2π periodic function y , which satisfy (2.36) or (2.37).

In an irrotational flow of infinite depth, we may take $b = 0$ (see the discussion following (2.5e)), whence (2.37) further simplifies to

$$y = \frac{1}{2} \frac{c^2}{g} \left(1 - \frac{1}{(1 + \mathcal{H}y')^2 + (y')^2} \right).$$

The result agrees with what Dyachenko *et al.* (1996a), for instance, derived.

Reformulation as an equation of Babenko kind

Unfortunately, (2.36) or (2.37) is not convenient for numerical computation because one would have to deal with rational functions of y . Moreover, Constantin *et al.* (2016) noted that (2.36) is not suitable for global bifurcation theory because it does not seem to make a compact operator. Below, we proceed along the same line as the argument in Constantin *et al.* (2016) to reformulate (2.36) as an equation of ‘‘Babenko kind.’’ It makes use of an extension of the Titchmarsh theorem to a strip (see (2.23)) for various quantities.

We begin by arranging (2.36) as

$$\begin{aligned} (c - \omega \mathcal{T}_d(y y'))^2 + 2(c - \omega \mathcal{T}_d(y y'))\omega y(1 + \mathcal{T}_d y') + \omega^2 y^2(1 + \mathcal{T}_d y')^2 \\ = (c^2 + 2b - 2g y)((1 + \mathcal{T}_d y')^2 + (y')^2), \end{aligned}$$

and rearranging as

$$\begin{aligned} (c - \omega \mathcal{T}_d(y y'))^2 + 2\omega y(c - \omega \mathcal{T}_d(y y'))(1 + \mathcal{T}_d y') - \omega^2 y^2 (y')^2 \\ = (c^2 + 2b - 2g y - \omega^2 y^2)((1 + \mathcal{T}_d y')^2 + (y')^2). \end{aligned} \quad (2.38)$$

An extension of the Titchmarsh theorem to a strip (see (2.23)) implies that $\mathcal{T}_d(y y') + i y y'$ makes the face value of a holomorphic and 2π periodic function in Σ_d , whose imaginary part is of mean zero at the face of Σ_d and vanishes at the bottom, and so does

$$(c - \omega(\mathcal{T}_d(y y') + i y y'))^2 = (c - \omega \mathcal{T}_d(y y'))^2 - \omega^2 y^2 (y')^2 - 2i(c - \omega \mathcal{T}_d(y y'))\omega y y'.$$

It then follows from (2.38) that

$$\begin{aligned}
& (c^2 + 2b - 2gy - \omega^2 y^2)((1 + \mathcal{T}_d y')^2 + (y')^2) \\
& \quad - 2\omega y(c - \omega \mathcal{T}_d(y y'))(1 + \mathcal{T}_d y') - 2i\omega y(c - \omega \mathcal{T}_d(y y'))y' \\
& = (c^2 + 2b - 2gy - \omega^2 y^2)((1 + \mathcal{T}_d y')^2 + (y')^2) - 2\omega y(c - \omega \mathcal{T}_d(y y'))(1 + \mathcal{T}_d y' + iy') \\
& = ((c^2 + 2b - 2gy - \omega^2 y^2)(1 + \mathcal{T}_d y' - iy') - 2\omega y(c - \omega \mathcal{T}_d(y y')))(1 + \mathcal{T}_d y' + iy')
\end{aligned} \tag{2.39}$$

is the face value of a holomorphic and 2π periodic function in Σ_d , whose imaginary part is of mean zero at the face of Σ_d and vanishes at the bottom.

Note that $1/(1 + \mathcal{T}_d y' + iy')$ is the face value of the holomorphic and 2π periodic function $= 1/z_u$ in Σ_d , whose imaginary part is of mean zero at the face of Σ_d and vanishes at the bottom. Indeed, z is holomorphic in Σ_d , $|z_u|^2 \neq 0$ in $\overline{\Sigma_d}$ by (2.11) and (2.10) and, moreover, $\langle \text{Im}(1/z_u) \rangle = 0$ for all $v \in [-d, 0]$ by the Cauchy-Riemann equations and (2.19d). Therefore, it follows from (2.39) that

$$(c^2 + 2b - 2gy - \omega^2 y^2)(1 + \mathcal{T}_d y' - iy') - 2\omega y(c - \omega \mathcal{T}_d(y y'))$$

is the face value of a holomorphic and 2π periodic function in Σ_d , whose imaginary part is of mean zero at the face of Σ_d and vanishes at the bottom. An extension of the Titchmarsh theorem to a strip (see (2.23)) then implies that

$$(c^2 + 2b - 2gy - \omega^2 y^2)(1 + \mathcal{T}_d y') - 2\omega y(c - \omega \mathcal{T}_d(y y')) = -\mathcal{T}_d((c^2 + 2b - 2gy - \omega^2 y^2)y')$$

up to an additive real constant. Or, equivalently,

$$\begin{aligned}
& (c^2 + 2b)\mathcal{T}_d y' - (g + c\omega)y - g(y\mathcal{T}_d y' + \mathcal{T}_d(y y')) \\
& \quad - \frac{1}{2}\omega^2(y^2 + y^2\mathcal{T}_d y' + \mathcal{T}_d(y^2 y') - 2y\mathcal{T}_d(y y')) = \mu,
\end{aligned}$$

say. An integration over the periodic interval $[-\pi, \pi]$ reveals that

$$\mu = -g\langle y(1 + \mathcal{T}_d y') \rangle - c\omega\langle y \rangle - \frac{1}{2}\omega^2\langle y^2 \rangle.$$

Indeed, $\langle \mathcal{T}_d f' \rangle = 0$ for any function f by (2.20) and, moreover, since $f \mapsto \mathcal{T}_d f'$ is self-adjoint,

$$\langle y^2 \mathcal{T}_d y' \rangle = \frac{1}{2\pi} \int_{-\pi}^{\pi} y^2 \mathcal{T}_d y' \, du = -\frac{1}{2\pi} \int_{-\pi}^{\pi} y \mathcal{T}_d(y^2)' \, du = -\langle 2y \mathcal{T}_d(y y') \rangle.$$

To recapitulate,

$$\begin{aligned}
& (c^2 + 2b)\mathcal{T}_d y' - (g + c\omega)y - g(y\mathcal{T}_d y' + \mathcal{T}_d(y y')) \\
& \quad - \frac{1}{2}\omega^2(y^2 + y^2\mathcal{T}_d y' + \mathcal{T}_d(y^2 y') - 2y\mathcal{T}_d(y y')) \\
& \quad + g\langle y(1 + \mathcal{T}_d y') \rangle + c\omega\langle y \rangle + \frac{1}{2}\omega^2\langle y^2 \rangle = 0.
\end{aligned} \tag{2.40}$$

In the infinite depth, the periodic Hilbert transform replaces \mathcal{T}_d .

We emphasize that (2.40) is made up of polynomials of y (involving its derivative and \mathcal{T}_d), whence it is straightforward to implement in numerical computation. It is the subject of investigation here. Moreover, Constantin *et al.* (2016) verified that the linearization of (2.40) with respect to y and b is a compact operator in a suitable function space, provided that $c^2 + 2b - 2y > 0$ pointwise in \mathbb{R} , whereby they established a global bifurcation result.

But for any $\omega \in \mathbb{R}$, $d \in (0, \infty]$ and $b, c \in \mathbb{R}$,

$$\begin{aligned}
& y \mapsto (c^2 + 2b)\mathcal{T}_d y' - (g + c\omega)y - g(y\mathcal{T}_d y' + \mathcal{T}_d(y y')) \\
& \quad - \frac{1}{2}\omega^2(y^2 + \mathcal{T}_d(y^2 y') + y^2\mathcal{T}_d y' - 2y\mathcal{T}_d(y y')) + g\langle y(1 + \mathcal{T}_d y') \rangle + c\omega\langle y \rangle + \frac{1}{2}\omega^2\langle y^2 \rangle
\end{aligned}$$

maps 2π periodic functions to 2π periodic functions of mean zero, whereas

$$y \mapsto (c + \omega y(1 + \mathcal{T}_d y') - \omega \mathcal{T}_d(y y'))^2 - (c^2 + 2b - 2gy)((1 + \mathcal{T}_d y')^2 + (y')^2)$$

maps 2π periodic functions to 2π periodic functions, not necessarily of mean zero. In other words, (2.40) and (2.36) agree except a constant. It is because $\mathcal{T}_d + i$ makes the face value of a holomorphic and 2π periodic function in Σ_d merely up to an additive real constant. In order to reconcile loss of information from (2.36) to (2.40), we require that the solutions of (2.40) in addition satisfy

$$\langle (c + \omega y(1 + \mathcal{T}_d y') - \omega \mathcal{T}_d(y y'))^2 \rangle = \langle (c^2 + 2b - 2gy)((1 + \mathcal{T}_d y')^2 + (y')^2) \rangle. \quad (2.41)$$

Consequently, (2.40) and (2.41) are equivalent to (2.36).

Furthermore, (2.36) cannot uniquely determine y and b , and neither can (2.40) and (2.41). It is because (2.5) is a free boundary problem. Indeed, b depends on the location of the coordinates of the fluid region, among others. Recall (2.27), and we assume, without loss of generality, that

$$\langle y(1 + \mathcal{T}_d y') \rangle = 0; \quad (2.42)$$

y then measures the fluid surface displacement from zero and h the mean fluid depth. It in turn simplifies (2.40).

We assume in addition that the solutions of (2.40), (2.41) and (2.42) are even. Indeed, for arbitrary vorticity, under some assumptions, Hur (2007) and Constantin *et al.* (2007), among others, proved that a Stokes wave is a priori symmetric about the crest.

To summarize, the Stokes wave problem, permitting constant vorticity and finite depth, is to find a vorticity $\omega \in \mathbb{R}$, a mean conformal depth $d \in (0, \infty]$, a ‘‘Bernoulli constant’’ $b \in \mathbb{R}$, a wave speed $c \in \mathbb{R}$, and a 2π periodic and even function y , measuring the fluid surface displacement from zero, which satisfy

$$\begin{aligned} (c^2 + 2b)\mathcal{T}_d y' - (g + c\omega)y - g(y\mathcal{T}_d y' + \mathcal{T}_d(y y')) \\ - \frac{1}{2}\omega^2(y^2 + \mathcal{T}_d(y^2 y') + y^2 \mathcal{T}_d y' - 2y\mathcal{T}_d(y y')) + c\omega \langle y \rangle + \frac{1}{2}\omega^2 \langle y^2 \rangle = 0 \end{aligned} \quad (2.43a)$$

and

$$\langle (c + \omega y(1 + \mathcal{T}_d y') - \omega \mathcal{T}_d(y y'))^2 \rangle - \langle (c^2 + 2b - 2gy)((1 + \mathcal{T}_d y')^2 + (y')^2) \rangle = 0. \quad (2.43b)$$

We usually regard ω and d as prescribed, and y and b as the unknowns, depending on the parameter c , although we at times switch the roles of c and ω or d ; see Section 3.2, Section 4.3 and Section 4.4, for instance. In the finite depth, we determine the mean fluid depth h by solving (2.12), depending on the solution. One may instead fix h and determine d as part of the solution.

We remark that Constantin *et al.* (2016) focused on steady waves to discover (2.43), and here we begin by deriving the governing equations in the unsteady wave setting and rediscover (2.43) by seeking the steady solutions, which is potentially useful for addressing stability and other unsteady wave phenomena. It is a subject of future investigation. Moreover, Constantin *et al.* (2016) required $\langle y \rangle = 0$ in place of (2.42). But we infer from (2.27) that (2.42) is more suitable for studying unsteady waves.

In an irrotational flow, (2.43a) simplifies to

$$(c^2 + 2b)\mathcal{T}_d y' - gy - g(y\mathcal{T}_d y' + \mathcal{T}_d(y y')) = 0. \quad (2.44)$$

Moreover, we may redefine the square of the wave speed $= c^2 + 2b$ so long as it is positive. Therefore, for zero vorticity, the Stokes wave problem is to find $d \in (0, \infty]$, $c^2 + 2b \in (0, \infty)$ and a 2π periodic and even function y , which satisfy (2.44). The result agrees with what

Dyachenko *et al.* (1996*a,b*), for instance, derived. In stark contrast, for nonzero constant vorticity, one must determine b as part of the solution by solving (2.43*a*) and (2.43*b*) simultaneously for y and b .

In the infinite depth, in addition, the periodic Hilbert transform replaces \mathcal{T}_d and we may take $b = 0$ (see the discussion following (2.5*e*)), whence (2.44) further simplifies to

$$c^2 \mathcal{H}y' - gy - g(y\mathcal{H}y' + \mathcal{H}(yy')) = 0. \quad (2.45)$$

Longuet-Higgins (1978) proposed a collection of infinitely many equations for the Fourier coefficients of a Stokes wave, which Babenko (1987) rediscovered in the form of (2.45), and, independently, Plotnikov (1992); Dyachenko *et al.* (1996*a*); Buffoni *et al.* (2000*a,b*), among others. One may regard (2.43) as to extending the Babenko equation to permit constant vorticity and finite depth.

We compare (2.43*a*) and (2.44) to learn that nonzero constant vorticity adds higher order nonlinearities to the equation, whence it may contribute to new wave phenomena. In stark contrast, we compare (2.44) and (2.45) to learn that the mean conformal depth merely changes the scaling factor of the Fourier multiplier in the equation, whence it would not influence the qualitative properties of the solutions. The result from the present numerical computation bears it out.

3. Numerical method

We begin by writing (2.43) in the operator form as

$$F(y, b; c, \omega, d) = 0, \quad (3.1)$$

where $F(y, b; c, \omega, d) = (Y, B)(y, b; c, \omega, d)$,

$$\begin{aligned} Y(y, b; c, \omega, d) = & (c^2 + 2b)\mathcal{T}_d y' - (g + c\omega)y - g(y\mathcal{T}_d y' + \mathcal{T}_d(yy')) \\ & - \frac{1}{2}\omega^2(y^2 + \mathcal{T}_d(y^2 y')) + y^2 \mathcal{T}_d y' - 2y\mathcal{T}_d(yy') + c\omega\langle y \rangle + \frac{1}{2}\omega^2\langle y^2 \rangle \end{aligned} \quad (3.2a)$$

and

$$B(y, b; c, \omega, d) = \langle (c + \omega y(1 + \mathcal{T}_d y') - \omega \mathcal{T}_d(yy'))^2 \rangle - \langle (c^2 + 2b - 2gy)((1 + \mathcal{T}_d y')^2 + (y')^2) \rangle. \quad (3.2b)$$

For any $b, c, \omega \in \mathbb{R}$ and $d \in (0, \infty]$, $Y(\cdot, b; c, \omega, d)$ maps 2π periodic and even functions to 2π periodic and even functions, whence

$$Y(y, b; c, \omega, d)(u) = \sum_{k \in \mathbb{Z}} \widehat{Y}(k)(y, b; c, \omega, d) e^{iku} \quad \text{for } u \in \mathbb{R}$$

in the Fourier series, where

$$\begin{aligned} \widehat{Y}(k)(y, b; c, \omega, d) = & \frac{1}{2\pi} \int_{-\pi}^{\pi} ((c^2 + 2b)\mathcal{T}_d y' - (g + c\omega)y - g(y\mathcal{T}_d y' + \mathcal{T}_d(yy')) \\ & - \frac{1}{2}\omega^2(y^2 + \mathcal{T}_d(y^2 y')) + y^2 \mathcal{T}_d y' - 2y\mathcal{T}_d(yy')) e^{iku} du \end{aligned} \quad (3.3a)$$

and $\widehat{Y}(k) = \widehat{Y}(-k)$ for all $k \in \mathbb{Z}$. In what follows, we identify Y with $(\widehat{Y}(0), \widehat{Y}(1), \widehat{Y}(2), \dots)$. Note that

$$\widehat{Y}(0)(y, b; c, \omega, d) = \langle y(1 + \mathcal{T}_d y') \rangle. \quad (3.3b)$$

3.1. Newton-GMRES method

Suppose that

$$y^{(n+1)} = y^{(n)} + \delta y^{(n)} \quad \text{and} \quad b^{(n+1)} = b^{(n)} + \delta b^{(n)} \quad \text{for } n = 0, 1, 2, \dots \quad (3.4)$$

solve (3.1) and (3.3)-(3.2b) iteratively by the Newton method, where $y^{(0)}$ and $b^{(0)}$ make an initial guess, to be supplied (see Section 3.2 for details), $\delta y^{(n)}$ and $\delta b^{(n)}$ solve

$$\delta F(y^{(n)}, b^{(n)}; c, \omega, d)(\delta y^{(n)}, \delta b^{(n)}) = -F(y^{(n)}, b^{(n)}; c, \omega, d), \quad (3.5)$$

$F(y^{(n)}, b^{(n)}; c, \omega, d)$ is defined in (3.3)-(3.2b), and $\delta F(y^{(n)}, b^{(n)}; c, \omega, d)$ is the linearization of $F(y, b; c, \omega, d)$ with respect to y and b , and evaluated at $y = y^{(n)}$ and $b = b^{(n)}$. We use (3.3) and (3.2b), and we make an explicit calculation to show that

$$\delta F(y, b; c, \omega, d)(\delta y, \delta b) = (\delta \widehat{Y}(0), \delta \widehat{Y}(1), \delta \widehat{Y}(2), \dots, \delta B)(y, b; c, \omega, d)(\delta y, \delta b),$$

where

$$\begin{aligned} \delta \widehat{Y}(k)(y, b)(\delta y, \delta b) &= \frac{1}{2\pi} \int_{-\pi}^{\pi} ((c^2 + 2b)\mathcal{T}_d(\delta y)' + 2\delta b\mathcal{T}_d y' - (g + c\omega)\delta y \\ &\quad - g(\delta y\mathcal{T}_d y' + y\mathcal{T}_d(\delta y)' + \mathcal{T}_d(y\delta y)') \\ &\quad - \frac{1}{2}\omega^2(2y\delta y + \mathcal{T}_d(y^2\delta y)' - [2y\delta y, y] + [y^2, \delta y]))e^{iku} du \end{aligned} \quad (3.6a)$$

for $k = 1, 2, \dots$, $[f_1, f_2] := f_1\mathcal{T}_d f_2' - f_2\mathcal{T}_d f_1'$,

$$\delta \widehat{Y}(0)(y, b)(\delta y, \delta b) = \langle \delta y + 2y\mathcal{T}_d(\delta y)' \rangle \quad (3.6b)$$

and

$$\begin{aligned} \delta B(y, b)(\delta y, \delta b) &= 2\omega \langle (c + \omega y(1 + \mathcal{T}_d y') - \omega\mathcal{T}_d(y y')) \\ &\quad \times (\delta y(1 + \mathcal{T}_d y') + y\mathcal{T}_d(\delta y)' - \mathcal{T}_d(y\delta y)') \rangle \\ &\quad - 2 \langle (\delta b - g\delta y)((1 + \mathcal{T}_d y')^2 + (y')^2) \rangle \\ &\quad - 2 \langle (c^2 + 2b - 2gy)((1 + \mathcal{T}_d y')\mathcal{T}_d(\delta y)' + y'(\delta y)') \rangle. \end{aligned} \quad (3.6c)$$

We approximate $y^{(n)}$ by a truncated Fourier series and, by abuse of notation, let

$$y^{(n)}(u) := \sum_{k=-N/2}^{N/2-1} \widehat{y^{(n)}}(k)e^{iku} \quad (3.7)$$

for some even N , where $\widehat{y^{(n)}}(k) = \widehat{y^{(n)}}(-k)$ for all $k \in \mathbb{Z}$, by symmetry. We approximate $\widehat{y^{(n)}}(k)$ by a discrete Fourier transform and, by abuse of notation, let

$$\widehat{y^{(n)}}(k) := \frac{1}{N} \sum_{j=0}^{N-1} y^{(n)}(u_j)e^{iku_j} \quad \text{for } k = -N/2, \dots, N/2 - 1, \quad (3.8)$$

where

$$u_j = -\pi + 2\pi j/N \quad \text{for } j = 0, 1, \dots, N-1 \quad (3.9)$$

make uniform grid points of the periodic interval $[-\pi, \pi]$, and $y^{(n)}(u_j) = y^{(n)}(u_{N-j})$ for $j = 0, 1, \dots, N/2 - 1$, by symmetry. We compute (3.8) using a fast Fourier transform (FFT). We numerically approximate $\mathcal{T}_d(y^{(n)})'$ (see (2.20)) and polynomial nonlinearities, e.g. $y^{(n)}\mathcal{T}_d(y^{(n)})'$, likewise, using (3.7)-(3.9), an FFT and the inverse FFT.

Together, we numerically approximate (3.5), using (3.7)-(3.9), an FFT and the inverse, by

$$\begin{aligned} & (\delta\widehat{Y}(0), \delta\widehat{Y}(1), \dots, \delta\widehat{Y}(N/2-1), \delta B)(y^{(n)}, b^{(n)}; c, \omega, d)(\delta y^{(n)}, \delta b^{(n)}) \\ & = -(\widehat{Y}(0), \widehat{Y}(1), \dots, \widehat{Y}(N/2-1), B)(y^{(n)}, b^{(n)}; c, \omega, d), \end{aligned} \quad (3.10)$$

where $\widehat{Y}(0), \widehat{Y}(1), \dots, \widehat{Y}(N/2-1), B$ are in (3.3)-(3.2b), and $\delta\widehat{Y}(0), \delta\widehat{Y}(1), \dots, \delta\widehat{Y}(N/2-1), \delta B$ in (3.6); $y^{(n)}$ is in (3.7) and $\delta y^{(n)}$, likewise; N is the number of the Fourier coefficients or, alternatively, the number of the grid points in (3.7)-(3.9). By the way, $(\delta\widehat{Y}(0), \delta\widehat{Y}(1), \dots, \delta\widehat{Y}(N/2-1), \delta B)(y^{(n)}, b^{(n)}; c, \omega, d)$ is not given explicitly, but for any $(\delta y^{(n)}, \delta b^{(n)})$, the left side of (3.10) may be computed using an FFT and a pseudo-spectral method.

It is reasonable to solve (3.10) by a Krylov subspace method. Some excellent surveys include Greenbaum (1997); Meurant (1999); Saad (2003); Simoncini & Szyld (2007). But the conjugate gradient (CG) method does not seem to converge for strong positive vorticity, among others. The conjugate residual (CR) and minimal residual (MINRES) methods are better but unreliable. Perhaps, it is because for any $c, \omega \in \mathbb{R}$ and $d \in (0, \infty]$,

$$\begin{aligned} (\delta y, \delta b) \mapsto & (c^2 + 2b)\mathcal{T}_d(\delta y)' + 2\delta b\mathcal{T}_d y' - (g + c\omega)\delta y \\ & - g(\delta y\mathcal{T}_d y' + y\mathcal{T}_d(\delta y)' + \mathcal{T}_d(y\delta y)') - \frac{1}{2}\omega^2(2y\delta y + \mathcal{T}_d(y^2\delta y)' - [2y\delta y, y] + [y^2, \delta y]), \end{aligned}$$

where $[f_1, f_2] = f_1\mathcal{T}_d f_2' - f_2\mathcal{T}_d f_1'$, and, hence, (3.6a) are not self-adjoint. In stark contrast, for any $b \in \mathbb{R}$, for any $c, \omega \in \mathbb{R}$ and $d \in (0, \infty]$,

$$\begin{aligned} \delta y \mapsto & (c^2 + 2b)\mathcal{T}_d(\delta y)' - (g + c\omega)\delta y \\ & - g(\delta y\mathcal{T}_d y' + y\mathcal{T}_d(\delta y)' + \mathcal{T}_d(y\delta y)') - \frac{1}{2}\omega^2(2y\delta y + \mathcal{T}_d(y^2\delta y)' - [2y\delta y, y] + [y^2, \delta y]) \end{aligned}$$

is self-adjoint. Indeed, in an irrotational flow of infinite depth, where we may take $b = 0$, the CG or CR method does converge; see Dyachenko *et al.* (2016); Lushnikov (2016); Lushnikov *et al.* (2017), for instance.

For nonzero constant vorticity, the generalized minimal residual (GMRES) method (see Saad & Schultz 1986, for instance) turns out to converge in the least number of iterates, compared with the CG, CR and MINRES methods. The result reported herein is based on the GMRES method. By the way, one may instead attempt to solve

$$(\delta F)^*(\delta F)(y^{(n)}, b^{(n)}; c, \omega, d)(\delta y^{(n)}, \delta b^{(n)}) = -(\delta F)^* F(y^{(n)}, b^{(n)}; c, \omega, d)$$

by the CG or CR method, where the asterisk denotes the adjoint. It is presently under investigation.

We emphasize that an FFT computes a discrete Fourier transform in $O(N \log N)$ operations, where N is the number of the Fourier coefficients or, alternatively, the number of the grid points (see (3.7)-(3.9)). To compare, a boundary integral method in Simmen & Saffman (1985); Teles da Silva & Peregrine (1988), for instance, would compute a numerical solution in $O(N^2)$ operations, although a customized \sqrt{N} grid points would possibly improve it to $O(N)$.

A uniform grid is clearly not very effective for nearly extreme waves, whose crests tend to sharpen and troughs flatter. In an irrotational flow of infinite depth, Lushnikov *et al.* (2017), for instance, proposed an auxiliary conformal mapping, which adapts the numerical points for high curvature so that an FFT computes a discrete Fourier transform in $O(\sqrt{N} \log N)$ operations in the auxiliary conformal variable for comparable resolution. In Section 4.2, we exercise the idea for nonzero constant vorticity in the infinite depth.

3.2. Initial guess

It turns out that we must supply $y^{(0)}$ and $b^{(0)}$ sufficiently close to a true solution of (3.1) and (3.3)-(3.2b), in order for the Newton-GMRES method in the previous subsection to converge.

For $\omega \in \mathbb{R}$ and $d \in (0, \infty]$ prescribed, we begin by taking $\omega = 0$, $d = \infty$ and a Padé approximation of a Stokes wave, in practice, of small amplitude:

$$z(w) \sim w + iy_0 + \sum_{m=1}^M \frac{\gamma_m}{\tan(w/2) - i\beta_m} \quad \text{for } w = u + iv \in \mathbb{C},$$

where $z(u + iv)$ for $v < 0$ is the conformal mapping from the lower half plane of \mathbb{C} to the fluid region, $z(u + i0)$ is the fluid surface (see (2.6)), and $z(u + iv)$ for $v > 0$ is an analytic continuation of the conformal mapping to the upper half plane of \mathbb{C} ; β_m and γ_m for $m = 1, 2, \dots, M$ for some M are the poles and residues of the Padé approximation, and y_0 is chosen so that (2.42) holds. See Dyachenko *et al.* (2016), for instance, for details. By the way, z is holomorphic in the lower half plane of \mathbb{C} but it may admit singularities in the upper half plane. A library of β_m and γ_m from zero to a nearly maximum amplitude is found in Dyachenko *et al.* (2015), for instance, which enables one to reconstruct Stokes waves, in an irrotational flow of infinite depth, for the relative error less than 10^{-26} .

We then continue the numerical solution along in ω and d , taking the prior convergent solution as the initial guess and solving (3.1) and (3.3)-(3.2b) by the method in the previous subsection, until we reach a solution for the desired values of ω and d . One may instead recall the Stokes wave expansion; see Simmen & Saffman (1985); Teles da Silva & Peregrine (1988), for instance.

To proceed, we fix ω and d , and continue the numerical solution along in c , taking the prior convergent solution as the initial guess and solving (3.1) and (3.3)-(3.2b) by the method in Section 3.1. But there is a caveat. For strong positive vorticity, the solution curve in the wave speed versus amplitude plane turns out to experience a ‘‘gap’’ of unphysical solutions; see Figure 3 and Figure 5, for instance. For stronger positive vorticity, the maximum wave speed in the gap becomes considerably larger and, hence, the number of steps in c one would have to take to continue along and trace out the gap. For instance, for $\omega = 2.25$ and $d = 1$ (see Figure 5), the wave speed reaches the order of hundreds in the gap. It is then more effective to continue the physical solution along in ω (and c) from a smaller value of ω .

3.3. Convergence

For a numerical solution $y^{(n)}$ and $b^{(n)}$ of (3.1) and (3.3)-(3.2b), we define the residual as

$$\text{res}(y^{(n)}, b^{(n)}) = \sum_{k=-N/2}^{N/2-1} |\hat{Y}(k)(y^{(n)}, b^{(n)})|^2 + |B(y^{(n)}, b^{(n)})|^2,$$

where N is the number of the Fourier coefficients in the numerical approximation (see (3.7)-(3.9)). It measures how far $y^{(n)}$ and $b^{(n)}$ are from a true solution of (3.1) and (3.3)-(3.2b). We say that the Newton method converges if

$$\text{res}(y^{(n)}, b^{(n)}) < \sqrt{N}10^{-13}. \quad (3.11)$$

But if the wave speed of a numerical solution is of the order of hundreds (see Figure 5, for instance), we necessarily relax (3.11) to

$$\text{res}(y^{(n)}, b^{(n)}) < \sqrt{N}10^{-9}. \quad (3.12)$$

For a numerical solution $\delta y^{(n)}$ and $\delta b^{(n)}$ of (3.5)-(3.6) or, equivalently, (3.10), we define the residual likewise as

$$\begin{aligned} \delta \text{res}(\delta y^{(n)}, \delta b^{(n)}) &= \sum_{k=-N/2}^{N/2-1} |\delta \widehat{Y}(k)(y^{(n)}, b^{(n)})(\delta y^{(n)}, \delta b^{(n)}) + \widehat{Y}(k)(y^{(n)}, b^{(n)})|^2 \\ &\quad + |\delta B(y^{(n)}, b^{(n)})(\delta y^{(n)}, \delta b^{(n)}) + B(y^{(n)}, b^{(n)})|^2. \end{aligned}$$

Because (3.5)-(3.6) is to better approximate the numerical solutions of (3.1) and (3.3)-(3.2b), we do not have to insist the residual of (3.5)-(3.6) smaller than a fraction of that of (3.1) and (3.3)-(3.2b). As Yang (2010), for instance, suggested, we say that the GMRES method converges if

$$\delta \text{res}(\delta y^{(n)}, \delta b^{(n)}) < \epsilon \text{res}(y^{(n)}, b^{(n)}) \quad (3.13)$$

for some small ϵ , say, 0.01. To compare, Simmen & Saffman (1985) and Vanden-Broeck (1996) required the residuals less than 10^{-11} , and Teles da Silva & Peregrine (1988) the residuals less than 10^{-10} .

In the present computation, the number of the Newton iterates remains constant as N increases from 256 to $2^{16} = 65536$ and it rarely takes more than 12, in order for a numerical solution of (3.1) and (3.3)-(3.2b) to satisfy (3.11). The number of the GMRES iterates, on the other hand, varies from the order of tens to thousands for N in the range, in order for a numerical solution of (3.5)-(3.6) to satisfy (3.13).

3.4. Error

Lastly, we require that a numerical solution $y^{(n)}$ (and $b^{(n)}$) of (3.1) and (3.3)-(3.2b) satisfies

$$|\widehat{y^{(n)}}(N/2)| < 10^{-12}, \quad (3.14)$$

where N is the number of the Fourier coefficients in the numerical approximation, so that the truncation error in (3.7) is insignificant. In general, we have to take N considerably larger for higher waves, in order to accurately resolve the numerical solutions. Indeed, in an irrotational flow of infinite depth, if one requires that a numerical solution satisfies

$$|\widehat{y^{(n)}}(N/2)| < N^{-1/2} 10^{-26}$$

in place of (3.14), then $N = 256$ for the steepness = 0.0994457, but $N = 2^{27} \approx 1.3 \times 10^8$ in order to estimate the steepness of the wave of greatest height up to 32 digits; see Dyachenko *et al.* (2016), for instance. In the present computation, we take N in the range of 256 to $2^{16} = 65536$, and we do not attempt to find a solution if it requires more than 2^{16} Fourier coefficients to satisfy (3.14), because it takes too much time.

4. Result

If y , b and c make a solution of (2.43) or, equivalently, (3.1) and (3.3)-(3.2b) for some ω and d , then it is straightforward to verify that so do y , b and $-c$ for $-\omega$ and d . In what follows, we assume that c is positive and, in turn, allow that ω be either positive or negative, representative of waves propagating upstream or downstream, respectively; see Teles da Silva & Peregrine (1988), for instance.

We take $g = 1$ for simplicity. Recall that the period is 2π . The steepness s measures the crest-to-trough height divided by 2π .

4.1. Finite depth

Throughout the subsection, $d = 1$ for simplicity.

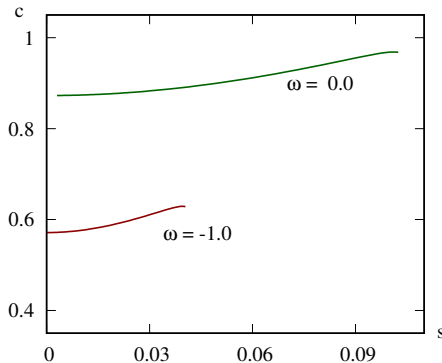


FIGURE 1. Wave speed versus steepness for $d = 1$, $\omega = 0$ (green) and $\omega = -1$ (red).

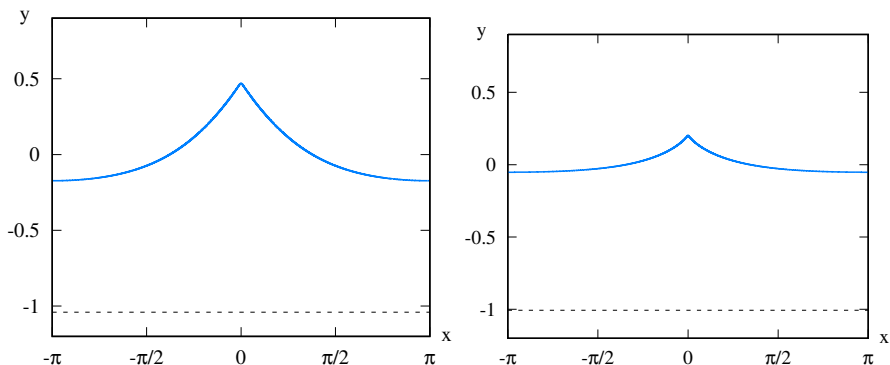


FIGURE 2. (left) For $\omega = 0$ and $d = 1$, the wave profile in the (x, y) plane of the solution at the end point of the $c = c(s)$ curve in Figure 1. (right) For $\omega = -1$ and $d = 1$, the wave profile of the solution at the end point of the solution curve in Figure 1. The mean fluid surface is at $y = 0$ and the mean fluid depths are marked by dashed lines.

Zero or negative vorticity

We begin by taking $\omega = 0$, and numerically solve (3.1) and (3.3)-(3.2b) using the method in the previous section. Figure 1 includes the wave speed versus steepness from the result. It resembles the well-known result in an irrotational flow of infinite depth; see the inset of Figure 6, for instance.

The left panel of Figure 2 displays the wave profile of the numerical solution at the end point of the $c = c(s)$ curve in Figure 1, in the (x, y) plane for $x \in [-\pi, \pi]$, for which calculated are $c = 0.9679$, $s = 0.1024$ and $h = 1.0398$. The mean fluid surface is at $y = 0$. Clearly, it is near an *extreme wave*, which exhibits a sharp corner at the crest. Like in the infinite depth (see Longuet-Higgins & Fox 1978, for instance), we conjecture that c experiences infinitely many oscillations and s increases monotonically toward the extreme wave. But the numerical solutions beyond the end point of the $c = c(s)$ curve in Figure 1 require more than $2^{16} = 65536$ Fourier coefficients to satisfy (3.14), whence we do not compute them. We note that h varies little throughout the $c = c(s)$ curve.

For $\omega = -1$, in Figure 1 is the wave speed versus steepness. It resembles the result for $\omega = 0$. In the right panel of Figure 2 is the wave profile of the numerical solution at the end point of the $c = c(s)$ curve; $c = 0.6285$, $s = 0.0404$ and $h = 1.0286$. The steepness is noticeably less than for $\omega = 0$.

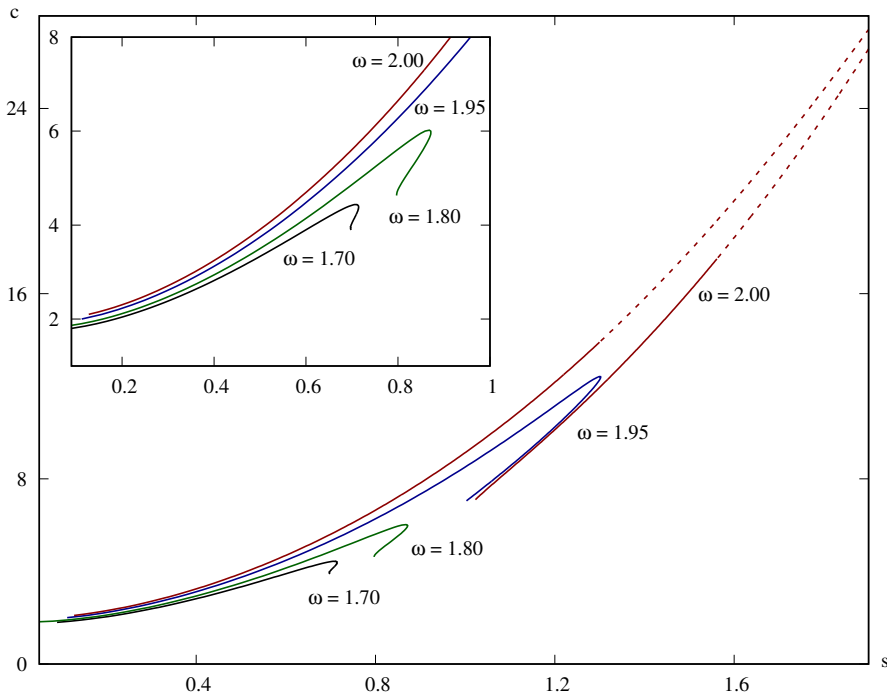


FIGURE 3. Wave speed versus steepness for $d = 1$, $\omega = 1.7$ (black), 1.8 (green), 1.95 (blue) and 2 (red). Solid curves physical solution, and the dashed curve unphysical solution. The inset is a closeup of the $c = c(s)$ curves for $s < 1$.

We verify what Teles da Silva & Peregrine (1988) obtained, using a boundary integral method. For instance, for $\omega = -1$ and $h = 1$, (Teles da Silva & Peregrine 1988, Figure 3(a)) reports a solution for $c = 0.5883$ and the crest-to-trough height = 0.12. We find one for $c = 0.5883$ and the crest-to-trough height = 0.1201, $d = 0.9978$.

We may carry out the numerical computation for other values of negative vorticity. We predict that the result resembles that for $\omega = 0$ or -1 . See Simmen & Saffman (1985), for instance, for some details, but for $d = \infty$. We predict that the crest becomes lower for stronger negative vorticity.

Positive vorticity

For weak positive vorticity, the result resembles that for zero or negative vorticity (see Simmen & Saffman (1985), for instance, for some details for $d = \infty$), but not for strong positive vorticity. Figure 3 includes the wave speed versus steepness for several values of positive vorticity.

For $\omega = 1.7$, the inset of Figure 3 reveals that the steepness increases, decreases and then increases along the $c = c(s)$ curve. Namely, a *fold* develops. Consequently, there correspond two or three solutions for some s . We predict that the continuation of the solution is limited by an extreme wave, which seems no longer the wave of greatest height. We note that there are no overhanging profiles throughout the $c = c(s)$ curve.

Figure 3 indicates that the fold increases in size as ω increases. Moreover, waves observedly become more rounded for stronger positive vorticity. In particular, for $\omega = 1.95$, we find an overhanging wave, whose profile is no longer the graph of a single valued function.

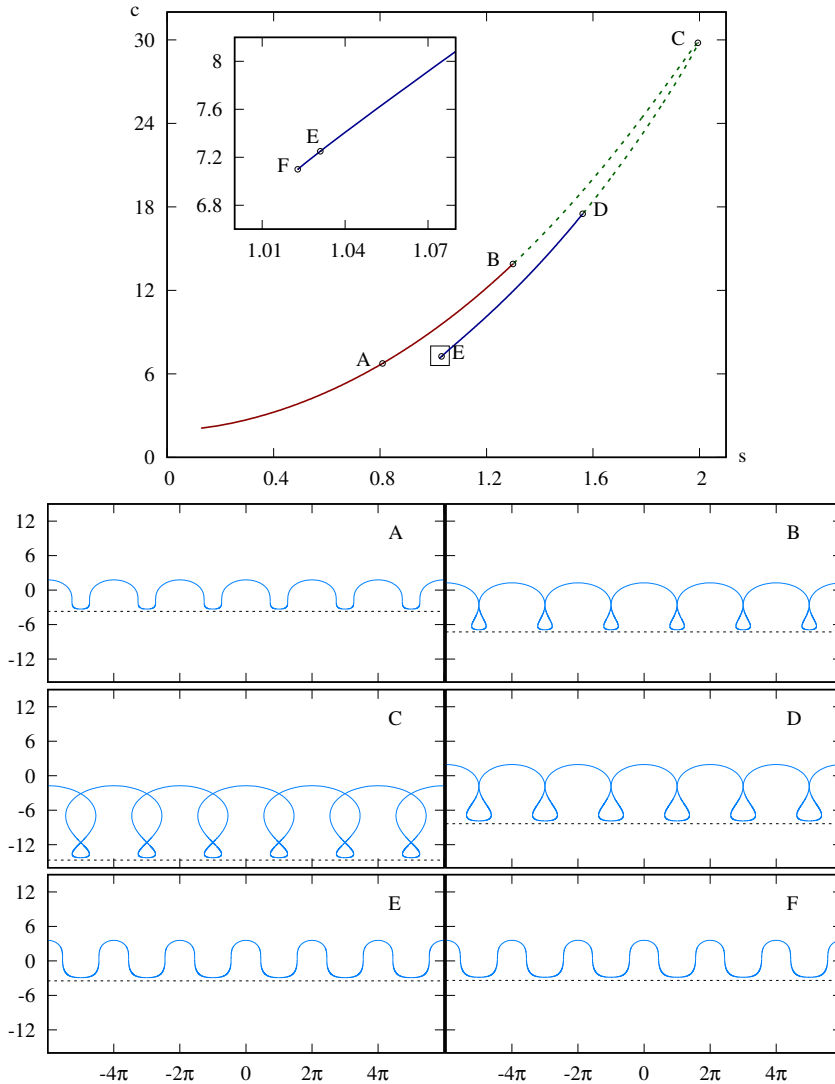


FIGURE 4. (top) Wave speed versus steepness for $\omega = 2$ and $d = 1$. The inset is a closeup near the end point of the numerical continuation. (bottom) Wave profiles of the solutions labelled by A through F . The mean fluid surface is at $y = 0$ and the mean fluid depths are marked by dashed lines.

For $\omega = 2$, the top panel of Figure 4 (see also Figure 3) shows the wave speed versus steepness. We continue the solution along the $c = c(s)$ curve from zero to a *touching wave*, whose profile self-intersects somewhere along the trough line, trapping an air bubble. Beyond such a limiting wave, the numerical solution becomes unphysical because the fluid surface in the conformal variable, $u \mapsto (u + \mathcal{T}_d y(u), y(u))$, (see (2.25)) is no longer injective for $u \in [-\pi, \pi]$. We continue the unphysical solution along the fold of the $c = c(s)$ curve, to reach another touching wave, and beyond such a limiting wave, the numerical solution becomes physical. Therefore, a *gap* of unphysical solutions develops in the $c = c(s)$ curve, which is limited by touching waves. We remark that the numerical

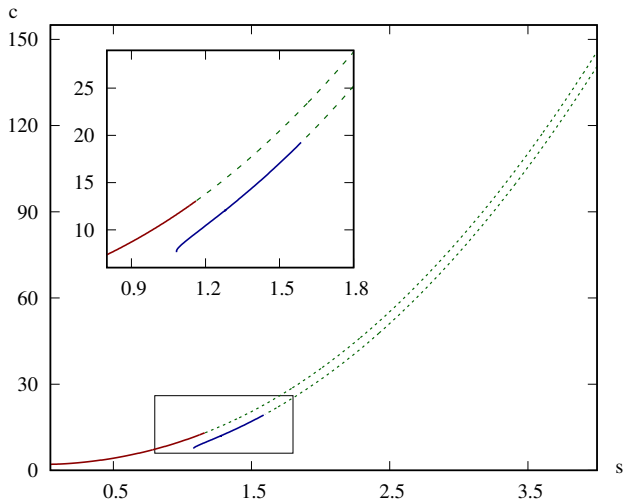


FIGURE 5. Wave speed versus steepness for $\omega = 2.25$ and $d = 1$. The inset is a closeup near the limiting waves.

method in Simmen & Saffman (1985), for instance, diverges in the gap. In stark contrast, the present numerical method converges throughout the $c = c(s)$ curve.

The bottom panel of Figure 4 displays six profiles along the $c = c(s)$ curve: $s = 0.8092$, $h = 3.6882$; $s = 1.2997$, $h = 7.2563$; $s = 1.9939$, $h = 1.4664$; $s = 1.5615$, $h = 8.3509$; $s = 1.0310$, $h = 3.4647$; $s = 1.0228$, $h = 3.3992$, respectively.

Wave *A* is single valued and *B* is near a touching wave. By the way, it resembles a limiting capillary wave. Overhanging occurs somewhere between waves *A* and *B*. Wave *C* is in the gap, whose steepness is the maximum. It is unphysical because the fluid region over one period overlaps adjacent ones. Wave *D* is near another touching wave. We find that wave *D* traps a larger air bubble than *B*. Wave *E* is single valued. We find that waves become more rounded from zero to wave *C* and less rounded beyond *C*, so that overhanging ultimately disappears toward the extreme wave. Wave *F* is at the end point of the $c = c(s)$ curve in the top panel, beyond which the numerical solutions require more than $2^{16} = 65536$ Fourier coefficients for accurate resolution. We note that h varies wildly along the $c = c(s)$ curve.

Moreover, we find that the gap increases in size as ω increases. For instance, for $\omega = 2.25$, Figure 5 reveals that the wave speed reaches the order of hundreds in the gap. To compare, for $\omega = 2$ (see Figure 4), the wave speed does not exceed 30. By the way, for $\omega = 2.25$, we discontinue the numerical solution at $c = 220$ and allow (3.12) in place of (3.11) in the gap. In order to locate a solution in the branch from a touching wave to an extreme wave of the $c = c(s)$ curve, without tracing out the gap, we begin by taking $\omega = 2$ and a physical solution in the touching-to-extreme branch, and continue it along in ω toward $\omega = 2.25$ while c is held fixed.

To summarize, the fold develops around $\omega = 1.7$, and increases in size as ω increases. Overhanging waves appear for some ω in the range 1.8 to 1.95. The gap develops for some ω in the range 1.95 to 2, and becomes larger as ω increases.

For stronger positive vorticity, we predict that one continues the solution from zero to a touching wave, which marks the outset of a gap; across the gap is another touching wave, which encloses a larger air bubble; one continues the solution through a fold until one reaches an extreme wave.

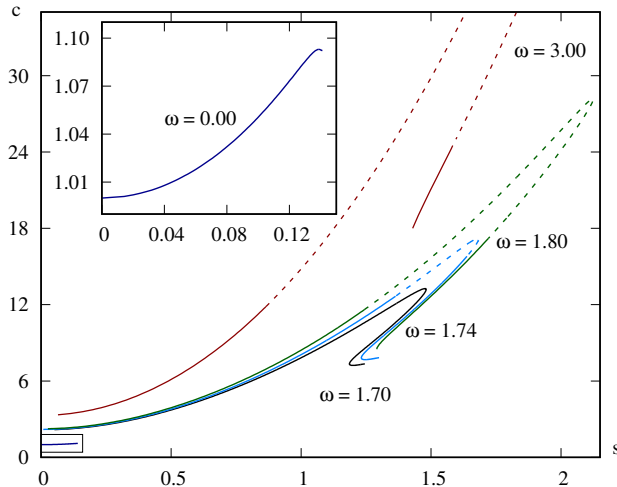


FIGURE 6. Wave speed versus steepness for $d = \infty$, $\omega = 0$ (blue), 1.7 (black), 1.8 (green) and 3 (red). Solid curves for physical solution, and dashed curves for unphysical solution. The inset is a closeup of the $c = c(s)$ curve for $\omega = 0$.

4.2. Infinite depth

We turn the attention to $d = \infty$. For zero vorticity, Lushnikov *et al.* (2017) proposed an auxiliary conformal mapping: for $\lambda > 0$,

$$w(\zeta) = 2 \arctan \left(\lambda \tan \frac{\zeta}{2} \right), \quad \text{where } \zeta = \xi + i\eta \quad \text{and} \quad w = u + iv, \quad (4.1)$$

conformally maps the lower half plane of \mathbb{C} of 2π period in the ξ variable to the lower half plane of \mathbb{C} of 2π period in the u variable and, moreover, $w \rightarrow \pm\pi$ as $\zeta \rightarrow \pm\pi$.

Since $u \sim \lambda\xi$ for $\lambda \ll 1$, (4.1) maps uniform grid points in the ξ variable to non-uniform in the u variable, concentrating them near $u = 0$ by a factor of λ and spreading them out near $u = \pm\pi$ by a factor of $1/\lambda$. Moreover, an FFT computes a discrete Fourier transform in $O(\sqrt{N})$ operations in the ξ variable, whereas it takes $O(N)$ operations in the u variable, where N is the number of grid points over one period. It is particularly effective for nearly extreme waves, whose crests tend to sharpen and troughs flatter. For instance, in an irrotational flow of infinite depth, a uniform grid in the u variable requires $2^{27} \approx 1.3 \times 10^8$ Fourier coefficients to estimate the wave of greatest height up to 32 digits (see Dyachenko *et al.* 2016, for instance), whereas a uniform grid in the ξ variable and, hence, a non-uniform grid in the u variable use about 4.2×10^4 Fourier coefficients (see Lushnikov *et al.* 2017) for comparable resolution.

The result in the subsection makes use of (4.1) for nonzero constant vorticity. Unfortunately, to the best of the authors' knowledge, no such mapping is known in the finite depth. It is an interesting question for future investigation.

Figure 6 includes the wave speed versus steepness for several values of vorticity. It agrees with (Simmen & Saffman 1985, Figure 9), using a boundary integral method. By the way, the vorticity in Simmen & Saffman (1985) differs in sign. Moreover, it resembles the result in the finite depth; see Figure 3. Indeed, Figure 7 indicates that the effects of depth are merely to change steepness and other quantities, and they are insignificant otherwise. We note that greater depths allow larger waves for higher speeds.

For $\omega = 0$, the inset of Figure 6 reproduces the well-known result of Longuet-Higgins & Fox (1978), among others, that single valued profiles tend to an extreme wave as the steepness

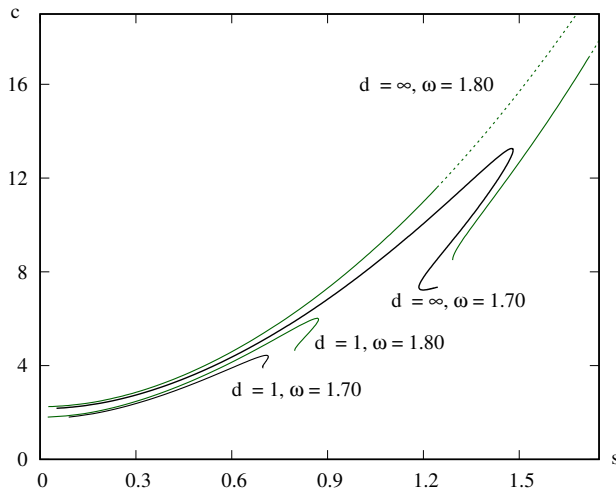


FIGURE 7. Wave speed versus steepness for $d = 1$ (green) and ∞ (black) for $\omega = 1.7$ and 1.8 .

increases monotonically. See also Lushnikov *et al.* (2017), among others. Like in the previous subsection in the finite depth, the fold develops for some ω in the range 1.3 to 1.5, and increases in size as ω increases. Overhanging waves appear for some ω in the range 1.6 to 1.7. The gap develops around $\omega = 1.7$, and becomes larger as ω increases. See Simmen & Saffman (1985) for more details.

For $\omega = 3$, there seems to correspond two, one or zero solutions for some s less than the maximum. By the way, like in the previous subsection in the finite depth, we discontinue the numerical solution at c at the order of hundreds, and locate a solution in the touching-to-extreme branch of the $c = c(s)$ curve by continuing along in ω from a smaller value.

Figure 8 displays the wave speed versus steepness for $\omega = 1.74$ and a selection of wave profiles along the $c = c(s)$ curve. The middle panel is, qualitatively and quantitatively, in excellent agreement with (Simmen & Saffman 1985, Figure 8). The bottom panel shows the wave profile of the numerical solution in the gap of the $c = c(s)$ curve, labelled by X , for which calculated are $c = 16.4$ and $s = 1.6139$. Clearly, it is unphysical. By the way, the numerical method in Simmen & Saffman (1985), for instance, diverges in the gap.

4.3. Large vorticity limit

Throughout the subsection, $d = \infty$.

In Figure 9, we begin by taking $\omega = 4.3$ and wave A in the gap close to the touching-to-extreme branch of the $c = c(s)$ curve, for which $c = 34.0$. We take wave A as the initial guess and continue the solution along in ω and c , to reach wave B , for which $\omega = 5.5$ and $c = 36.0$. We continue the solution along in ω and c , likewise, to reach waves C and D ; $\omega = 7.6$, $c = 48.5$ and $\omega = 14.0$, $c = 51.7$, respectively. We note that waves B , C and D are in the touching-to-extreme branches of the $c = c(s)$ curves. They become more rounded for stronger vorticity, and the trough becomes wider. Consequently, a *neck* develops in the profile, which decreases in size as ω increases. We note that waves B , C and D resemble the profiles in (Figure 5 Vanden-Broeck 1996, for instance) at the zero gravity limit.

Figure 10 displays the wave speed versus steepness for $\omega = 14$ and a selection of wave profiles along the $c = c(s)$ curve. Wave A is near the end point of the zero-to-touching branch of the $c = c(s)$ curve. Wave B is near the outset of the touching-to-extreme branch,

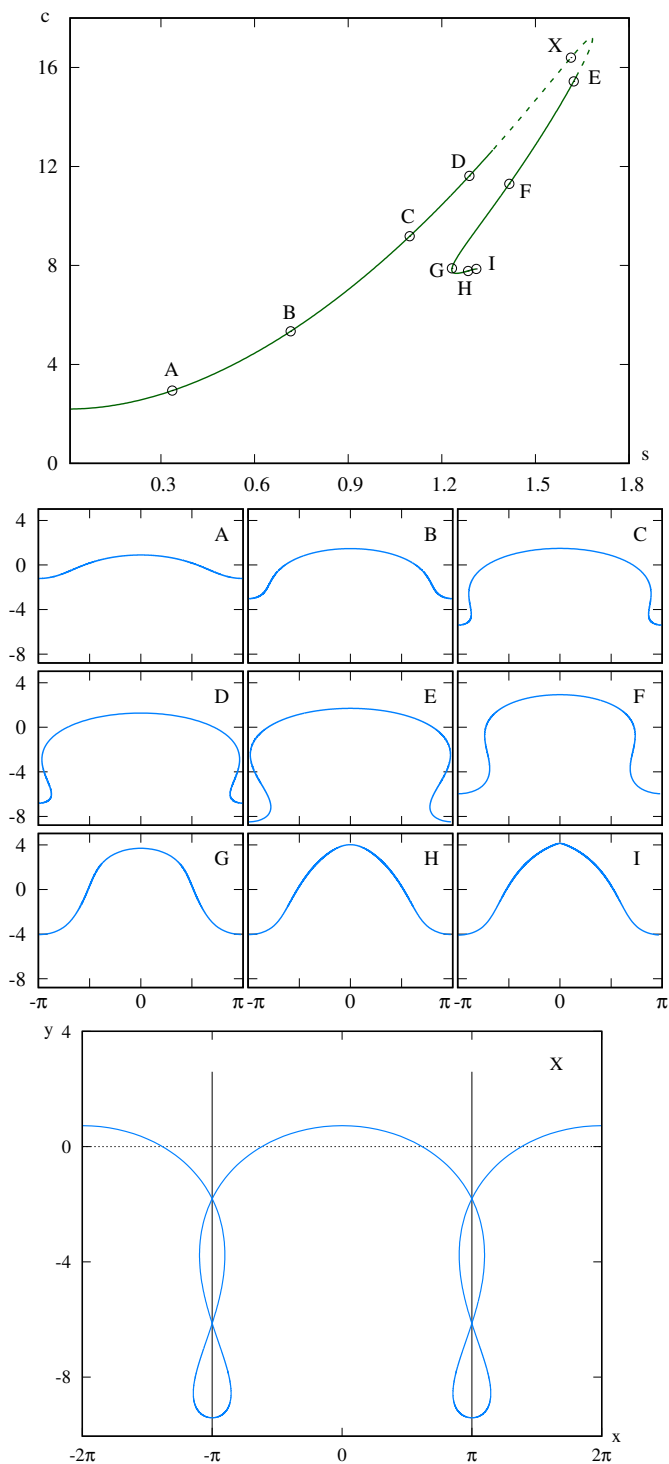


FIGURE 8. (top) Wave speed versus steepness for $\omega = 1.74$ and $d = \infty$. (middle) Wave profiles of the solutions labelled by A through I. The mean fluid surface is at $y = 0$. (bottom) Wave profile of the solution labelled by X in Figure 8.

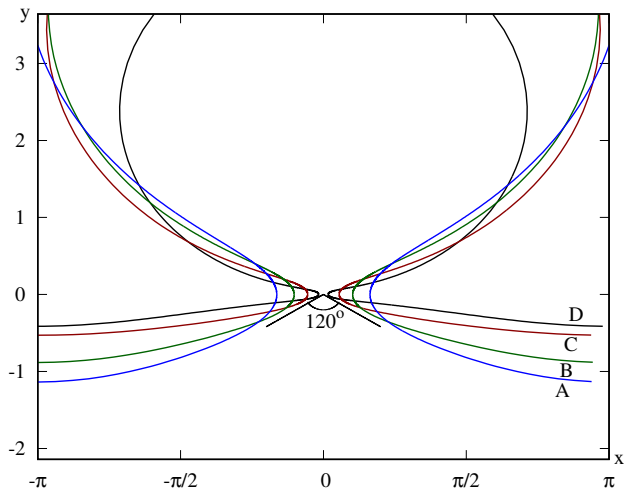


FIGURE 9. Wave profiles of the solutions for $d = \infty$, $\omega = 4.3$ and $c = 34.0$ (A, blue), $\omega = 5.5$ and $c = 36.0$ (B, green), $\omega = 7.6$ and $c = 48.5$ (C, red), and $\omega = 14.0$ and $c = 51.7$ (D, black).

and wave C is the end point of the $c = c(s)$ curve. Beyond wave C , the numerical solutions require more than $2^{16} = 65536$ Fourier coefficients for accurate resolution. Interestingly, the touching-to-extreme branch seems to intersect the gap. Wave D of Figure 9 seems located somewhere between waves B and C of Figure 10. By the way, we discontinue the numerical solution in the gap at $c \approx 250$, and locate wave B by continuing along in ω and c from smaller values.

We note that wave A closely resembles (Figure 4(b) Vanden-Broeck 1996, for instance) at the zero gravity limit. Dyachenko & Hur (2018) will study in detail the limiting wave at the end points of the zero-to-touching branches of the $c = c(s)$ curves as the strength of positive vorticity increases unboundedly or, equivalently, as gravitational acceleration vanishes.

We find that the neck decreases in size along the gap until it reaches a minimum, for which c is much less than a maximum, and then remains constant, particularly, from waves B to C . On the other hand, we note that waves become more rounded along the fold until c reaches the maximum, and then less rounded. Moreover, we note that the numerical solutions are ultimately limited by an extreme wave, which exhibits a sharp corner at the crest. Together, we predict that the “fluid bubble” disappears somewhere in the touching-to-extreme branch of the $c = c(s)$ curve.

Figure 9 reveals that the neck becomes narrower for stronger positive vorticity. Indeed, we predict that the minimum neck size vanishes as the strength of positive vorticity increases unboundedly. Moreover, we predict that the limiting wave at the large vorticity limit is rigid body rotation of a fluid disk. Dyachenko & Hur (2018) will confirm it.

4.4. Minimum depth limit

Lastly, we investigate a limit as the mean conformal depth decreases to the minimum. For instance, for $\omega = 3$ and $c = 6$ fixed, d decreases to ≈ 0.2193 . Figure 11 displays the wave profile of the numerical solution near such a minimum value, for which calculated is $h = 1.5329$. It resembles (Teles da Silva & Peregrine 1988, Figure 7(a)), for instance, whose trough is flat and limited by the fluid bed.

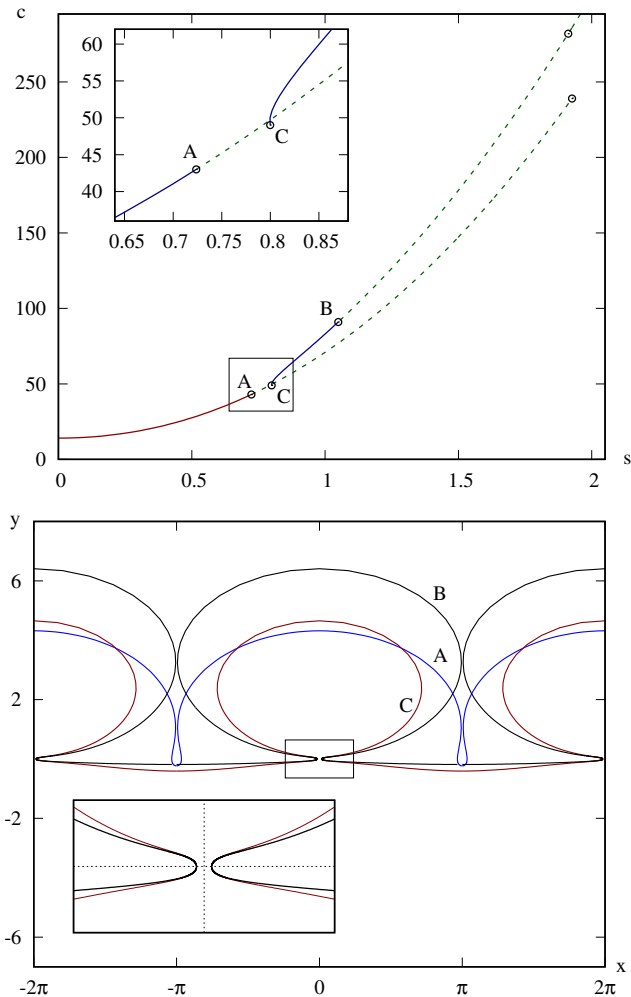


FIGURE 10. (top) Wave speed versus steepness for $\omega = 14$ and $d = \infty$. Solid curves for physical solution and dashed curves for unphysical solution. The inset is a closeup near the boundaries of the two solution branches. (bottom) Wave profiles of the solutions labelled by A, B and C. The inset is a closeup near the neck.

Acknowledgements

VMH is supported by the National Science Foundation under the Faculty Early Career Development (CAREER) Award DMS-1352597, an Alfred P. Sloan Research Fellowship, a Simons Fellowship in Mathematics, and by the University of Illinois at Urbana-Champaign under the Arnold O. Beckman Research Award RB14100. She is grateful to the Department of Mathematics at Brown University for its generous hospitality. SD is supported by the National Science Foundation Award DMS-1716822.

This material is based on work supported by the National Science Foundation under DMS-1439786 while the authors were in residence at the Institute for Computational and Experimental Research in Mathematics in Providence, RI, during the Spring 2017 semester.

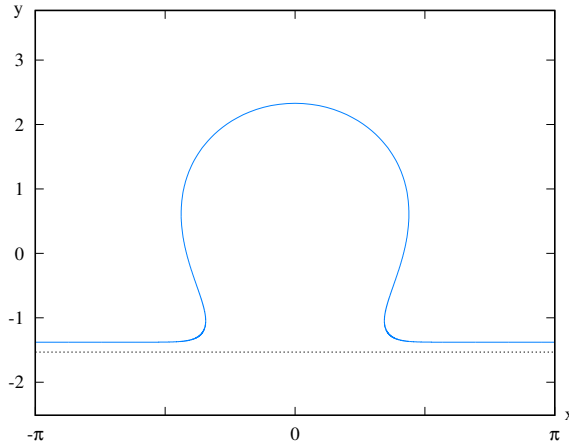


FIGURE 11. For $\omega = 3$ and $c = 6$, the wave profile near the minimum of the mean conformal depth. The mean fluid surface is $y = 0$ and the mean fluid depth is marked by the dashed line.

REFERENCES

- AMICK, C. J., FRAENKEL, L. E. & TOLAND, J. F. 1982 On the Stokes conjecture for the wave of extreme form. *Acta Math.* **148**, 193–214.
- BABENKO, K. I. 1987 Some remarks on the theory of surface waves of finite amplitude. *Soviet Math. Doklady* **35** (6), 599–603, (See also *loc. cit.* 647–650).
- BUFFONI, B., DANCER, E. N. & TOLAND, J. F. 2000a The regularity and local bifurcation of steady periodic water waves. *Arch. Ration. Mech. Anal.* **152** (3), 207–240.
- BUFFONI, B., DANCER, E. N. & TOLAND, J. F. 2000b The sub-harmonic bifurcation of Stokes waves. *Arch. Ration. Mech. Anal.* **152** (3), 241–271.
- CONSTANTIN, ADRIAN, EHRNSTRÖM, MATS & WAHLÉN, ERIK 2007 Symmetry of steady periodic gravity water waves with vorticity. *Duke Math. J.* **140** (3), 591–603.
- CONSTANTIN, ADRIAN & STRAUSS, WALTER 2004 Exact steady periodic water waves with vorticity. *Comm. Pure Appl. Math.* **57** (4), 481–527.
- CONSTANTIN, ADRIAN, STRAUSS, WALTER & VĂRĂRUCĂ, EUGEN 2016 Global bifurcation of steady gravity water waves with critical layers. *Acta Math.* **217** (2), 195–262.
- DYACHENKO, A. I., KUZNETSOV, E. A., SPECTOR, M. D. & ZAKHAROV, V. E. 1996a Analytical description of the free surface dynamics of an ideal fluid (canonical formalism and conformal mapping). *Physics Letters A* **221** (1), 73–79.
- DYACHENKO, A. I., ZAKHAROV, V. E. & KUZNETSOV, E. A. 1996b Nonlinear dynamics of the free surface of an ideal fluid. *Plasma Physics Reports* **22** (10), 829–840.
- DYACHENKO, SERGEY A. & HUR, VERA MIKYOUNG 2018 Stokes waves with constant vorticity: II. limiting waves. *Preprint*.
- DYACHENKO, S. A., LUSHNIKOV, P. M. & KOROTKEVICH, A. O. 2015 Library of Stokes waves. Published electronically at <http://stokeswave.org>.
- DYACHENKO, S. A., LUSHNIKOV, P. M. & KOROTKEVICH, A. O. 2016 Branch cuts of Stokes wave on deep water. Part I: Numerical solution and Padé approximation. *Stud. Appl. Math.* **137** (4), 419–472.
- GAKHOV, F. D. 1990 *Boundary Value Problems*. Dover Publications, Inc., New York, translated from the Russian, Reprint of the 1966 translation.
- GREENBAUM, ANNE 1997 *Iterative Methods for Solving Linear Systems, Frontiers in Applied Mathematics*, vol. 17. Society for Industrial and Applied Mathematics (SIAM), Philadelphia, PA.
- HUR, VERA MIKYOUNG 2006 Global bifurcation theory of deep-water waves with vorticity. *SIAM J. Math. Anal.* **37** (5), 1482–1521.
- HUR, VERA MIKYOUNG 2007 Symmetry of steady periodic water waves with vorticity. *Philos. Trans. R. Soc. Lond. Ser. A Math. Phys. Eng. Sci.* **365** (1858), 2203–2214.

- HUR, VERA MIKYOUNG 2011 Stokes waves with vorticity. *J. Anal. Math.* **113**, 331–386.
- KO, JOY & STRAUSS, WALTER 2008*a* Effect of vorticity on steady water waves. *J. Fluid Mech.* **608**, 197–215.
- KO, JOY & STRAUSS, WALTER 2008*b* Large-amplitude steady rotational water waves. *Eur. J. Mech. B Fluids* **27** (2), 96–109.
- LONGUET-HIGGINS, M. S. 1978 Some new relations between Stokes's coefficients in the theory of gravity waves. *J. Inst. Math. Appl.* **22** (3), 261–273.
- LONGUET-HIGGINS, M. S. & FOX, M. J. H. 1978 Theory of the almost-highest wave. II. Matching and analytic extension. *J. Fluid Mech.* **85** (4), 769–786.
- LUSHNIKOV, PAVEL M. 2016 Structure and location of branch point singularities for Stokes waves on deep water. *J. Fluid Mech.* **800**, 557–594.
- LUSHNIKOV, PAVEL M., DYACHENKO, SERGEY A. & SILANTYEV, DENIS A. 2017 New conformal mapping for adaptive resolving of the complex singularities of Stokes wave. *Proc. A.* **473** (2202), 20170198, 19.
- MEIRON, DANIEL I., ORSZAG, STEVEN A. & ISRAELI, MOSHE 1981 Applications of numerical conformal mapping. *J. Comput. Phys.* **40** (2), 345–360.
- MEURANT, G. 1999 *Computer Solution of Large Linear Systems, Studies in Mathematics and its Applications*, vol. 28. North-Holland Publishing Co., Amsterdam.
- OVSYANNIKOV, LEV V 1973 Dynamics of a fluid. *MA Lavrent'ev Institute of Hydrodynamics Sib. Branch USSR Ac. Sci* **15**, 104–125.
- PLEMELJ, JOSIP 1964 *Problems in the Sense of Riemann and Klein*. Interscience Publishers John Wiley & Sons Inc. New York-London-Sydney.
- PLOTNIKOV, P. I. 1992 Nonuniqueness of solutions of the problem of solitary waves and bifurcation of critical points of smooth functionals. *Math. USSR Izvestiya* **38** (2), 333–357.
- RIBEIRO, JR., ROBERTO, MILEWSKI, PAUL A. & NACHBIN, ANDRÉ 2017 Flow structure beneath rotational water waves with stagnation points. *J. Fluid Mech.* **812**, 792–814.
- SAAD, YOUSEF 2003 *Iterative Methods for Sparse Linear Systems*, 2nd edn. Society for Industrial and Applied Mathematics, Philadelphia, PA.
- SAAD, YOUSEF & SCHULTZ, MARTIN H. 1986 GMRES: a generalized minimal residual algorithm for solving nonsymmetric linear systems. *SIAM J. Sci. Statist. Comput.* **7** (3), 856–869.
- TELES DA SILVA, A. F. & PEREGRINE, D. H. 1988 Steep, steady surface waves on water of finite depth with constant vorticity. *J. Fluid Mech.* **195**, 281–302.
- SIMMEN, J. A. & SAFFMAN, P. G. 1985 Steady deep-water waves on a linear shear current. *Stud. Appl. Math.* **73** (1), 35–57.
- SIMONCINI, VALERIA & SZYLD, DANIEL B. 2007 Recent computational developments in Krylov subspace methods for linear systems. *Numer. Linear Algebra Appl.* **14** (1), 1–59.
- STOKES, G. G. 1847 On the theory of oscillatory waves. *Trans. Camb. Philos. Soc.* **8**, 441–473.
- STOKES, G. G. 1880 *Mathematical and Physical Papers*, , vol. 1. Cambridge University Press.
- TANVEER, S. 1991 Singularities in water waves and Rayleigh-Taylor instability. *Proc. Roy. Soc. London Ser. A* **435** (1893), 137–158.
- TANVEER, S. 1993 Singularities in the classical Rayleigh-Taylor flow: formation and subsequent motion. *Proc. Roy. Soc. London Ser. A* **441** (1913), 501–525.
- TITCHMARSH, E. C. 1986 *Introduction to the Theory of Fourier Integrals*, 3rd edn. Chelsea Publishing Co., New York.
- VANDEN-BROECK, J.-M. 1996 Periodic waves with constant vorticity in water of infinite depth. *IMA J. Appl. Math.* **56** (2), 207–217.
- YANG, JIANKE 2010 *Nonlinear Waves in Integrable and Nonintegrable Systems, Mathematical Modeling and Computation*, vol. 16. Society for Industrial and Applied Mathematics (SIAM), Philadelphia, PA.
- ZAKHAROV, VLADIMIR E., DYACHENKO, ALEXANDER I. & VASILYEV, OLEG A. 2002 New method for numerical simulation of a nonstationary potential flow of incompressible fluid with a free surface. *Eur. J. Mech. B Fluids* **21** (3), 283–291.